

DTIC FILE COPY

(4)

RADC-TR-89-251  
Final Technical Report  
November 1989



AD-A217 413

## VELOCITY MATCHED OPTICAL TRANSMITTER

SUNY at Buffalo

Dr. Pao Lo Liu

DTIC  
S ELECTE D  
FEB 01 1990  
E

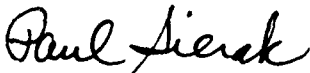
APPROVED FOR PUBLIC RELEASE; DISTRIBUTION UNLIMITED.


ROME AIR DEVELOPMENT CENTER  
Air Force Systems Command  
Griffiss Air Force Base, NY 13441-5700

9 0 0 2 0 1 0 6 7

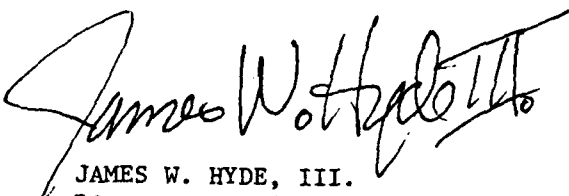
This report has been reviewed by the RADC Public Affairs Division (PA) and is releasable to the National Technical Information Services (NTIS). At NTIS it will be releasable to the general public, including foreign nations.

RADC-TR-89-251 has been reviewed and is approved for publication.

APPROVED:   
PAUL SIERAK  
Project Engineer

APPROVED:   
JOHN A. GRANIERO  
Technical Director  
Directorate of Communications

FOR THE COMMANDER:

  
JAMES W. HYDE, III.  
Directorate of Plans & Programs

If your address has changed or if you wish to be removed from the RADC mailing list, or if the addressee is no longer employed by your organization, please notify RADC (DCLW ) Griffiss AFB NY 13441-5700. This will assist us in maintaining a current mailing list.

Do not return copies of this report unless contractual obligations or notices on a specific document require that it be returned.

UNCLASSIFIED  
SECURITY CLASSIFICATION OF THIS PAGE

REPORT DOCUMENTATION PAGE				Form Approved OMB No 0704-0188	
1a. REPORT SECURITY CLASSIFICATION UNCLASSIFIED			1b. RESTRICTIVE MARKINGS N/A		
2a. SECURITY CLASSIFICATION AUTHORITY N/A			3. DISTRIBUTION/AVAILABILITY OF REPORT Approved for public release; distribution unlimited.		
2b. DECLASSIFICATION/DOWNGRADING SCHEDULE N/A			5. MONITORING ORGANIZATION REPORT NUMBER(S) RADC-TR-89-251		
4. PERFORMING ORGANIZATION REPORT NUMBER(S) N/A			7a. NAME OF MONITORING ORGANIZATION Rome Air Development Center (DCLW)		
6a. NAME OF PERFORMING ORGANIZATION SUNY at Buffalo		6b. OFFICE SYMBOL (If applicable) DCLW		7b. ADDRESS (City, State, and ZIP Code) Griffiss AFB NY 13441-5700	
6c. ADDRESS (City, State, and ZIP Code) Department of Computer & Electrical Engineering 215A Bonner Hall Amherst NY 14260		8a. NAME OF FUNDING/SPONSORING ORGANIZATION Rome Air Development Center		8b. OFFICE SYMBOL (If applicable) DCLW	
8c. ADDRESS (City, State, and ZIP Code) Griffiss AFB NY 13441-5700		9. PROCUREMENT INSTRUMENT IDENTIFICATION NUMBER F30602-81-C-0193			
10. SOURCE OF FUNDING NUMBERS					
PROGRAM ELEMENT NO 63726F		PROJECT NO 2863		TASK NO 92	
WORK UNIT ACCESSION NO P9					
11. TITLE (Include Security Classification) VELOCITY MATCHED OPTICAL TRANSMITTER					
12. PERSONAL AUTHOR(S) Dr. Pao Lo Liu					
13a. TYPE OF REPORT Final		13b. TIME COVERED FROM Jan 88 TO Dec 88		14. DATE OF REPORT (Year, Month, Day) November 1989	
15. PAGE COUNT 92					
16. SUPPLEMENTARY NOTATION N/A					
17. COSATI CODES			18. SUBJECT TERMS (Continue on reverse if necessary and identify by block number)		
FIELD	GROUP	SUB-GROUP			
17	02		External Optical Modulation		
17	08		Fiber Optic Modulators		
17	08		Lithium Niobate		
19. ABSTRACT (Continue on reverse if necessary and identify by block number) This report covers work towards development of a 50 GHz optical modulator. The H-guide configuration of the lithium niobate based modulator, along with the desire to reduce the modulation voltage, necessitated substrate dimensions of 1 cm x 120 $\mu$ m x 25 $\mu$ m. These dimensions were not obtainable. Polishing even below 25 $\mu$ m to reduce the modulation voltage proved unsuccessful. Obtaining the 120 $\mu$ m dimension after obtaining the 25 $\mu$ m dimension was also not obtainable. A new material for the structure is required which does not need mechanical processing to obtain the desired dimensions. This is the indicated path to pursue for obtaining a velocity matched modulator. Additionally, data is presented on V-shaped microcracks observed in titanium diffused lithium niobate presumed due to the heavy titanium indiffusion. Microcrack production leads to increased scattering and premature electrical breakdown.  Material is also presented on a computer aided design tool for optical waveguide devices.					
20. DISTRIBUTION/AVAILABILITY OF ABSTRACT <input checked="" type="checkbox"/> UNCLASSIFIED/UNLIMITED <input type="checkbox"/> SAME AS RPT. <input type="checkbox"/> DTIC USERS			21. ABSTRACT SECURITY CLASSIFICATION UNCLASSIFIED		
22a. NAME OF RESPONSIBLE INDIVIDUAL Paul Sierak			22b. TELEPHONE (Include Area Code) (315) 330-4092		22c. OFFICE SYMBOL RADC (DCLW)

DD Form 1473, JUN 86

Previous editions are obsolete.

SECURITY CLASSIFICATION OF THIS PAGE  
UNCLASSIFIED

# TABLE OF CONTENTS

Executive Summary	1
Chapter 1 Introduction	5
Chapter 2 Velocity-Matched Electrooptic Modulator	8
Chapter 3 Design and Layout of Waveguide Modulators	23
Chapter 4 Fabrication Tolerance of $\text{Ti:LiNbO}_3$ Waveguides	34
Chapter 5 Simulation of Electrooptic Effect on $\text{Ti:LiNbO}_3$ Modulators	56
Chapter 6 Fabrication of Velocity-Matched Optical Transmitter	71
Chapter 7 Surface Morphology of $\text{Ti:LiNbO}_3$ Waveguides	77
Conclusion	83

Accession For	
NTIS GRA&I	<input checked="" type="checkbox"/>
DTIC TAB	<input type="checkbox"/>
Unannounced	<input type="checkbox"/>
Justification	
By _____	
Distribution/	
Availability Codes	
Dist	Avail and/or Special
A-1	



## Executive Summary

The purpose of this project is to explore the possibility of using specially designed electrode structures to achieve velocity matching between optical signal and electrical modulation signal. With velocity matching condition met, the modulator can function in the 50 GHz region.

Due to the mechanical fragility of the substrate, we have not been able to finish a usable modulator.

Optoelectronic devices, such as, diode lasers, semiconductor detectors, fiber optics, and electrooptic waveguide modulators have been under extensive research and development during the past 15 years. They are building blocks for optical communications systems. Since the information capacity is directly related to the bandwidth, there are constantly ongoing efforts to improve the frequency response of these optoelectronic devices. Diode lasers have been demonstrated to operate at 28 GHz. Detectors with a bandwidth of 100 GHz have been fabricated and characterized. Waveguide modulators operating up to 22 GHz have been reported. With such broad bandwidths, they can readily be incorporated into microwave systems. Major advantages are: very low transmission loss at very high frequencies and essentially no crosstalk.

There are many potentially useful applications if we can modulate an optical beam at Q-band which is around 50 GHz. For example, we can establish new microwave links and design phased array radars using optical techniques. Because of these potential applications, we have been given the task of studying and implementing an optical transmitter which can be modulated at the Q-band.

We have indeed investigated all known approaches. The speed of diode lasers has reached its physical limit. The geometry of diode lasers has been optimized so that a low capacitance can be obtained. Various epitaxial layered structures, including, quantum well, have also been used to provide a higher speed. Modulators, however, have not reached their intrinsic limit. By matching the velocities of the modulation signal and the optical signal, the bandwidth of modulators is expected to increase.

Velocity matching condition can be met by considering the microwave properties of the electrodes. In the case of  $\text{Ti:LiNbO}_3$ , by using a series of coded electrode patterns, one can obtain modulation at 44 GHz. This approach, however, does not provide true velocity matching. It functions only at the designed center frequency. It does not provide modulation at dc and the modulation depth is also reduced. In the case of compound semiconductor waveguide modulator, there are indications by burying the electrodes between the semiconductor superstrate and substrate, one can obtain velocity matching. To our knowledge, such a device has not been experimentally characterized.

We have come up with a traveling-wave electrooptic modulator which can meet the velocity matching condition and function at 50 GHz region. From wave equations, we have obtained a closed-form solution demonstrating the operational principle. From the numerical values of the closed-form solution, we have found the design parameters. It requires a substrate width of 120  $\mu\text{m}$ . In order to reduce the modulation voltage, we have polished the substrate down to as thin as 25  $\mu\text{m}$ . With a 1 cm x 25  $\mu\text{m}$  x 120  $\mu\text{m}$  piece, the substrate is very fragile to handle. We have not been able to make a working modulator so far.

Progresses have been made in:

1. Establishing the operational principle and the design of a velocity-matched electrooptic modulator,
2. Establishing a fabrication facility for optoelectronic devices,
3. Developing fabricating processes for the velocity-matched electrooptic modulator.
4. Developing a routine running on microcomputer for the design and layout of waveguide modulators,
5. Developing a computer aided design tool which can provide modulation characteristics and fabrication tolerances of  $\text{Ti:LiNbO}_3$  waveguide modulators,
6. Studying the surface morphology of  $\text{Ti:LiNbO}_3$  waveguides for the first time by using confocal optical microscopy.

During this research, to aid in designing and fabricating waveguide modulators, we have also developed a computer aided design tool for photonic switches. We are the first to incorporate the electrooptic effect into the simulation program. Our calculate results show how variations in fabrication conditions can affect device performance. We are also the first to design and layout waveguide modulator patterns using a microcomputer. During the fabrication process, we have discovered an interesting phenomenon. After Ti-indiffusion, there is a V-shaped surface relief on the  $\text{LiNbO}_3$ . This is also the first time that such a relief has been observed. This surface feature can explain crack created when excess modulation voltage is applied. It may also affect the amount of light scattering in  $\text{LiNbO}_3$  waveguide devices, such as, the spectrum analyzer.

In summary, although we have established the operational principle and a device design, we have not been able to make the velocity-matched optical

transmitter because of the mechanical fragility of the substrate. We have made progresses in developing a computer aided design tool for photonic switches. We have developed a routine to design and layout waveguide modulator patterns on a microcomputer. We have also identified a surface relief which can explain the premature breakdown and excess light scattering in  $\text{LiNbO}_3$  waveguide devices.

Out of this research project, we have several papers published, submitted for publication, or under preparation:

1. Pao-Lo Liu, "Velocity-Matched Optical Transmitter," Proc. SPIE, vol. 995, 31 (1988).
2. F. S. Chu and P. L. Liu, "Simulation of Electrooptic Effect on  $\text{Ti:LiNbO}_3$  Modulators," submitted to IEEE J. Quantum Electron.
3. F. S. Chu and P. L. Liu, "Fabrication Tolerance of  $\text{Ti:LiNbO}_3$  Waveguides," submitted to J. Lightwave Tech.
4. M. Xu, P. C. Cheng, and P. L. Liu, "Surface Morphology of  $\text{Ti:LiNbO}_3$  Stripe Waveguides," to be presented in OSA Annual Meeting, 1989.
5. P. L. Liu, "Design and Layout of Optoelectronic Devices Using a Personal Computer," to be presented in OSA Annual Meeting, 1989.



## Chapter 1 Introduction

Optoelectronic devices, such as, diode lasers, semiconductor detectors, fiber optics, and electrooptic waveguide modulators have been under extensive research and development during the past 15 years. They are building blocks for optical communications systems. Since the information capacity is directly related to the bandwidth, there are constantly ongoing efforts to improve the frequency response of these optoelectronic devices. Diode lasers have been demonstrated to operate at 28 GHz. Detectors with a bandwidth of 100 GHz have been fabricated and characterized. Waveguide modulators operating up to 22 GHz have been reported. With such broad bandwidths, they can readily be incorporated into microwave systems. Indeed, there are analogue microwave links built using optoelectronic devices. Major advantages are: very low transmission loss at very high frequencies and essentially no crosstalk or interference.

There are many potentially useful applications if we can modulate an optical beam at Q-band which is around 50 GHz. For example, we can establish new microwave links and design phased array radars using optical techniques. In a conventional phased array radar, the phase of each radiating element must be precisely controlled. Using microwave phase shifters can be very clumsy. There are many delay lines that must be tuned and controlled. By using optoelectronic devices and circuits, we can control the phases with much shorter devices because we are dealing with optical wavelength. A phase change of  $360^\circ$  can be achieved by having an optical delay line of the order of a micron. In addition, we can also use a single beam deflecting device to encode the phases of all radiating elements. Because of these potential

advantages, we have been given the task of studying and implementing an optical transmitter which can be modulated at Q-band.

The speed of diode lasers has reached its physical limit. The geometry of diode lasers has been optimized so that a low capacitance can be obtained. Various epitaxial layered structures, including, quantum well, have also been used to provide a higher speed. Modulators, however, have not reached their intrinsic limit. By matching the velocities of the modulation signal and the optical signal, the bandwidth of modulators is expected to increase.

Velocity matching condition can be met by considering the microwave properties of the electrodes. In the case of  $\text{Ti:LiNbO}_3$ , by using a series of coded electrode patterns, one can obtain modulation at 44 GHz. This approach, however, does not provide true velocity matching. It functions only at the designed center frequency. It does not provide modulation at dc and the modulation depth is also reduced. In the case of compound semiconductor waveguide modulator, there are indications by burying the electrodes between the semiconductor superstrate and substrate, one can obtain velocity matching. To our knowledge, such a device has not been experimentally characterized.

In the following chapters of this report, we present results of our theoretical study on the design of a velocity-matched electrooptic modulator based on H-guide. We present the computer aided design tools that we developed to aid in waveguide device design and layout. To our best knowledge, we are the first to incorporate the electrooptic effect and the actual distribution of the modulation field into the beam propagation program. We also present our fabrication facility and actual fabrication

procedures as well as problems in the fabrication of the velocity-matched optical transmitter. A conclusion is presented at the end of this report.

## Chapter 2 Velocity-Matched Electrooptic Modulator

The intrinsic limitation of the bandwidth of electrooptic effect is set by lattice vibrations in the  $10^{12}$  Hz range. Currently, electrooptic devices are limited essentially by the electrodes. In the lumped capacitor configuration, the bandwidth of an electrooptic modulator is limited by the RC-charging time. Using a traveling-wave electrode, the bandwidth can be increased. However, because of the difference in the velocities of the optical signal and the microwave modulation signal, i.e., velocity mismatch, there is a walk-off problem which limits the bandwidth. In the case of  $\text{LiNbO}_3$ , the effective microwave index is 4.2 while the optical index is 2.2. There is a factor of, approximately, 2 difference in velocities. Reported devices have bandwidth in 6-22 GHz depending on the length of the devices. To further increase the bandwidth, we must overcome the velocity mismatch.

One possibility to overcome the velocity mismatch is to use the H-guide configuration. In an H-guide an electrooptic substrate, i.e.,  $\text{LiNbO}_3$ , is sandwiched between two conducting planar electrodes. The field of the modulation signal is distributed in the electrooptic substrate and in the surrounding space, i.e., air. The low dielectric constant of the surrounding space compensates the high dielectric constant of the substrate. By properly designing the devices, one can meet the velocity-matching requirement.

The H-guide was considered previously, however, only under the TEM approximation. This is adequate for low frequency modulation signals. But, it is not accurate for high frequency modulation signals. In the TEM approximation, the field of the modulation signal is essentially static. One can easily calculate the fraction of field in the electrooptic substrate and in the surrounding low index medium. By using an appropriate electrode

width, one can obtain an average index which meets the velocity matching requirement.

For high frequency applications, we must consider the field solutions of the H-guide. Indeed, we have done so. We find that it is possible to meet the velocity-matching condition. However, it is not through the adjustment of the electrode width. The H-guide is actually a microwave dielectric waveguide. The modulation field is guided by the electrooptic substrate. Outside of the substrate, the field decays exponentially. The width of this exponential tail is determined from the width and the dielectric constant of the substrate. By using an appropriate substrate width, we can indeed meet the velocity-matching condition. Once the velocity-matching condition is met, the only limitation is the ohmic loss of the planar electrode. Since we have hollow metallic waveguide operating in the Q-band, it shall not be a problem. The following is a manuscript summarizing the design of the velocity-matched electrooptic modulator.

# Velocity-Matched Optical Transmitter

Pao-Lo Liu

Department of Electrical and Computer Engineering

State University of New York at Buffalo

Amherst, N. Y. 14260

## ABSTRACT

The concept of using a low dielectric medium in a parallel-plate H-guide to obtain velocity-matching between optical and microwave signals for the  $\text{LiNbO}_3$  modulator is analyzed in detail. From solutions of the wave equations, we have obtained characteristics of the fundamental mode and the design parameters which lead to velocity-matching. The mode is guided by the electrooptic substrate and decays exponentially outside the  $\text{LiNbO}_3$  substrate. The parameter which determines its properties is  $2a/\lambda_0$ , i.e., width of the  $\text{LiNbO}_3$  substrate divided by the wavelength of the modulation signal. The phase velocity is dispersive, therefore, for a specific substrate width, velocity matching occurs only at a specific modulation frequency. A modulator built with such a velocity-matched electrode is expected to have only a finite bandwidth centered around the design frequency. Details of the analysis and characteristics of the H-guide are discussed in this paper.

## 1. INTRODUCTION

Electrooptic modulators based on the  $\text{LiNbO}_3$  suffers from the velocity mismatch, i.e., difference between the phase velocity of the modulation signal and the group velocity of the optical signal.<sup>1</sup> This limits the high frequency response of such modulators no matter whether they are bulk devices or integrated optical devices. In order to extend the high frequency response, several approaches have been considered. They can be classified into two categories: truly velocity-matched devices using low-dielectric constant medium in addition to the  $\text{LiNbO}_3$  and effectively velocity-matched devices using phase reversal electrodes at appropriate intervals.<sup>1-5</sup> The truly velocity-matched ones are expected to have the widest bandwidth.

The operational principle of the truly velocity-matched devices is simple. Since  $\text{LiNbO}_3$  has too high a dielectric constant, one can compensate it by partially filling electrodes with a low dielectric constant medium. The modulation field propagates in both the  $\text{LiNbO}_3$  and the low dielectric constant medium. An average dielectric constant which is determined by the fraction of the field in the  $\text{LiNbO}_3$  and the fraction of field in the low dielectric constant medium can be obtained. One example of such an approach is the H-guide.<sup>6</sup> The electrooptic substrate is placed at the center of a parallel plate electrode structure. By extending the electrodes beyond the width of the electrooptic substrate, part of the modulation field propagates in the surrounding low dielectric constant medium. By properly selecting the design parameters, one can obtain velocity matching. Indeed, an air-filled, velocity-matched bulk modulator was proposed and demonstrated.<sup>1</sup> The device was characterized up to few GHz. If an integrated optical version using the

thinned down substrate and the H-guide can be implemented, it shall have a wide bandwidth and a reasonably small modulation voltage.

In this paper, we consider the characteristics of the velocity-matched H-guide in detail. We present design parameters which can lead to the velocity matching. Different from the previous expectation, such a device is of the band-pass type because the phase velocity is dispersive.

## 2. THEORY

An H-guide is shown in Fig. 1. The electrooptic substrate is located at the center and is sandwiched between two perfect planar electrodes. In the waveguide version, the electrooptic substrate shall contain an optical waveguide, e.g., 6  $\mu\text{m}$ -wide Ti-indiffused waveguide. The permeability of the substrate at millimeter and submillimeter wavelengths is  $\epsilon_1$ . The permittivity is assumed to be  $\mu_1$ . The width of the substrate is  $2a$  and the height is  $b$ . The medium surrounding the substrate is characterized by  $\epsilon_2$  and  $\mu_2$ . The parallel plate electrodes are assumed to be infinite on the  $x$ - $z$  plane. The optical and the modulation signals propagate along the  $z$ -axis. In the case that we considered, the substrate is  $\text{LiNbO}_3$  and the surrounding medium is air. Therefore, we have  $\epsilon_1 = K_1 \epsilon_0$ ,  $\epsilon_2 = K_2 \epsilon_0$ , where  $K_1 = 34.7$ ,  $K_2 = 1$ , and  $\mu_1 = \mu_2 = \mu_0$ .

The properties of the H-guide can be analyzed by solving the wave equation with appropriate boundary conditions. Because of the symmetry, the guided electromagnetic wave can be categorized as either symmetric or asymmetric with respect to  $x=0$ . Furthermore, we can classify the supported modes into PE and PM. PE modes represent those with electric field lines



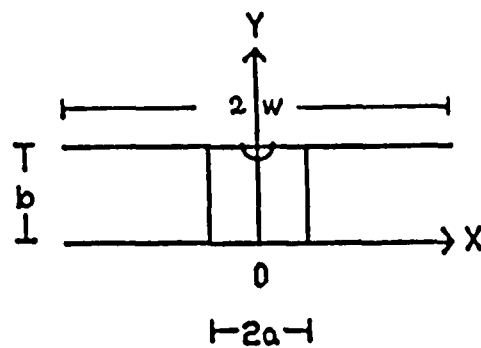


Fig. 1. The schematic diagram of an H-guide. An electrooptic substrate with width  $2a$  and thickness  $b$  is sandwiched between two perfect conducting planes acting as electrodes.

lying on planes parallel to the dielectric-air interface, i. e.,  $E_x=0$ . PM modes refer to those with magnetic field lines lying on planes parallel to the dielectric-air interface, i. e.,  $H_x=0$ . The boundary conditions are determined by field continuity at metallic boundaries,  $y=0$  and  $y=b$ , and dielectric boundaries,  $x=-a$ , and  $x=a$ . The metallic planes are assumed to be perfect conductors. The time and  $z$ -dependence of the field is assumed to be  $e^{j(\omega t - \beta z)}$ . Closed-form solutions of all field components have been obtained. It turns out that each mode can be labeled by a pair of integers,  $m$  and  $n$ .  $m$  is related to the boundary condition of the dielectric-air interface. The lowest order mode has an  $m$ -value of unity.  $n$  is related to the metallic boundaries and corresponds to the number of nodes along the  $y$ -direction. The minimum value of  $n$  is zero. Like other waveguide systems, the higher order modes can be pushed into cut-off by reducing the dimensions of the substrate. In fact, the  $mn$ -mode can only be supported if the substrate has a sufficient width and thickness:

$$a > (m-1)\lambda_0 / 4(K_1 - K_2)^{1/2}, \quad (1)$$

$$b > \frac{2\pi na}{[\pi^2 (2a/\lambda_0)^2 K_1 - (k_d a)^2]^{1/2}}, \quad (2)$$

where  $\lambda_0$  represents the vacuum wavelength of the modulation signal and  $k_d$  is the transverse wave vector in the substrate. By making  $a$  and  $b$  small, modes with  $m > 1$  or  $n > 0$  can all be eliminated. The lowest order mode which can propagate is  $PE_{10}$  mode. The next mode is  $PM_{11}$  mode.

The components of the  $E$ - and  $H$ -fields of the  $PE_{10}$  mode in the electrooptic substrate are:

$$E_{x1}=0, \quad (3)$$

$$E_{y1}=-A_1 \frac{\omega \mu_0}{k_d} \cos(k_d x), \quad (4)$$

$$E_{z1}=0, \quad (5)$$

$$H_{x1}=A_1 \frac{\beta^2}{\beta k_d} \cos(k_d x), \quad (6)$$

$$H_{y1}=0, \quad (7)$$

$$H_{z1}=jA_1 \sin(k_d x). \quad (8)$$

In the surrounding medium where  $x < -a$ , we have:

$$E_{x2}=0, \quad (9)$$

$$E_{y2}=-A_1 \frac{\omega \mu_0}{k_d} \cos(k_d a) e^{k_2(a+x)}, \quad (10)$$

$$E_{z2}=0, \quad (11)$$

$$H_{x2}=A_1 \frac{\beta^2}{\beta k_d} \cos(k_d a) e^{k_2(a+x)}, \quad (12)$$

$$H_{y2}=0, \quad (13)$$

$$H_{z2}=jA_1 \sin(k_d a) e^{k_2(a+x)}, \quad (14)$$

where  $A_1$  represents the amplitude of the field,  $\omega$  is its angular frequency, and  $k_2$  is the transverse wave vector in the surrounding medium. It is a symmetric TE mode. Because of the symmetry, we have only listed solutions in the  $x < -a$  portion of the surrounding medium. In the surrounding medium where  $x > a$ ,  $e^{k_2(a+x)}$  shall be replaced by  $e^{k_2(a-x)}$  and those terms which have a  $\sin(k_d a)$  dependence require a change in sign. The field is confined by the electrooptic substrate. Inside it, field components have a sinusoidal dependence. Outside the substrate, they decay exponentially away from the substrate. The decay rate is determined by  $k_2$ . To find  $k_2$ , one can use:

$$k_2 = k_d \tan(k_d a). \quad (15)$$

Such a transcendental equation comes from the boundary condition associated with the dielectric-air interface. It has a series of solutions. Each can be labeled with an integer  $m$ . Both  $k_d$  and  $k_2$  must be positive real numbers. Therefore, for the  $PE_{10}$  mode, we have  $0 \leq k_d a \leq \pi/2$ .  $k_d$  can be found from:

$$\pi^2 \left( \frac{2a}{\lambda_0} \right)^2 (K_1 - K_2) = \left[ \frac{k_d a}{\cos(k_d a)} \right]^2. \quad (16)$$

The longitudinal wave vector  $\beta$  is related to  $k_d$  or  $k_2$  by:

$$k_d^2 + \left( \frac{n\pi}{b} \right)^2 = \omega^2 \mu_0 \epsilon_0 K_1 - \beta^2, \quad (17)$$

$$k_2^2 - \left( \frac{n\pi}{b} \right)^2 = \beta^2 - \omega^2 \mu_0 \epsilon_0 K_2. \quad (18)$$

$\beta$  must be real. Otherwise, the wave becomes evanescent or un-guided.

Another parameter of great interest is the phase velocity. The effective relative phase velocity  $v_{\text{eff}}/c$  which is related to the longitudinal wave vector,  $\beta$ , can be calculated from Eq. (17). For the mn-mode, it is, assuming  $K_2=1$ ,:

$$v_{\text{eff}}/c = \frac{2\pi a/\lambda_0}{\left( \pi^2 \left( \frac{2a}{\lambda_0} \right)^2 \left[ K_1 - \left( \frac{n\lambda_0}{2b} \right)^2 \right] - (k_d a)^2 \right)^{1/2}} \quad (19)$$

### CALCULATED RESULTS

We have gone through the complete process of solving  $k_d$ ,  $k_2$ , and  $v_{\text{eff}}$  using  $2a/\lambda_0$  as the parameter. The  $PE_{10}$  mode does not have a cut-off, therefore, there is no restriction on the substrate width and thickness. Dependences of  $k_d a$ ,  $k_2 a$ , and  $v_{\text{eff}}/c$  versus  $2a/\lambda_0$  are shown in Figs. 2-4.

For  $\text{LiNbO}_3$ , the optical index of refraction is 2.2. Velocity matching can be achieved by choosing  $2a/\lambda_0 = 0.02$ . For 50 GHz operation, one needs a 120- $\mu\text{m}$  wide substrate. For 100 GHz operation, the width becomes 60  $\mu\text{m}$ . The corresponding values of  $k_d a$  and  $k_2 a$  are 0.344 and 0.123, respectively. The analysis is not limited to the  $\text{LiNbO}_3$ . In fact, for any electrooptic substrate and for any surrounding medium, one can follow the procedure and obtain the design condition for velocity matching.

It is interesting to note that the substrate thickness,  $b$ , doesn't play a role in the microwave characteristics of the structure. Therefore, one can use as thin a substrate as possible to reduce the modulation voltage or the switching power. It is essentially limited only by the mechanical strength of the substrate. A thickness of 25  $\mu\text{m}$  has been achieved. Thinner substrates, especially, polymer films may be realized in the future.

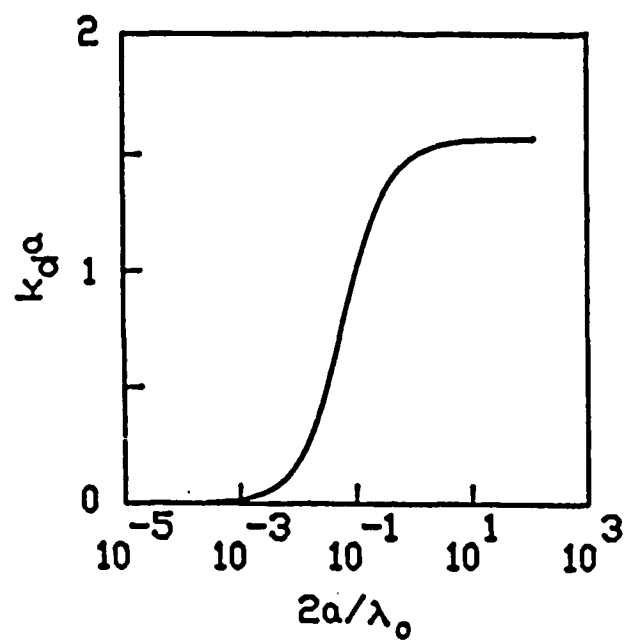


Fig. 2. The dependence of  $k_d a$  on  $2a/\lambda_0$  where  $k_d$  is the magnitude of the transverse wave vector inside the electrooptic substrate.

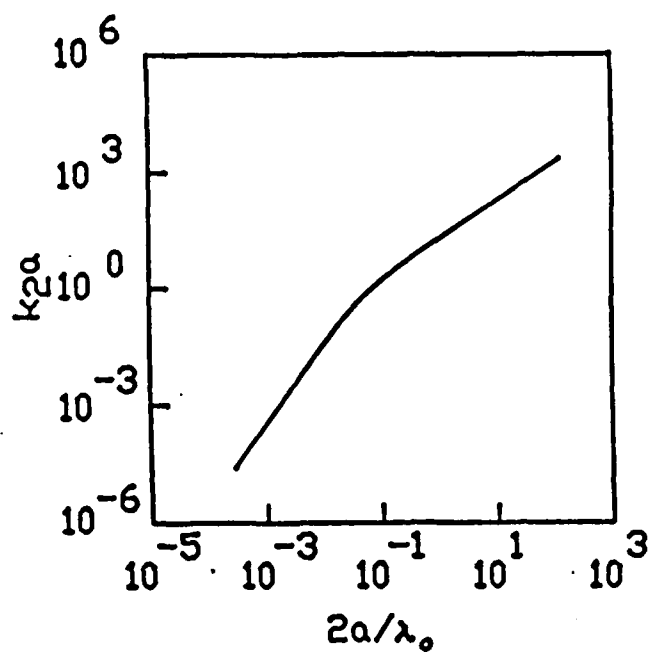


Fig. 3. The dependence of  $k_2 a$  on  $2a/\lambda_0$ .  $k_2$  determines the exponential decay of the field outside the electrooptic substrate.

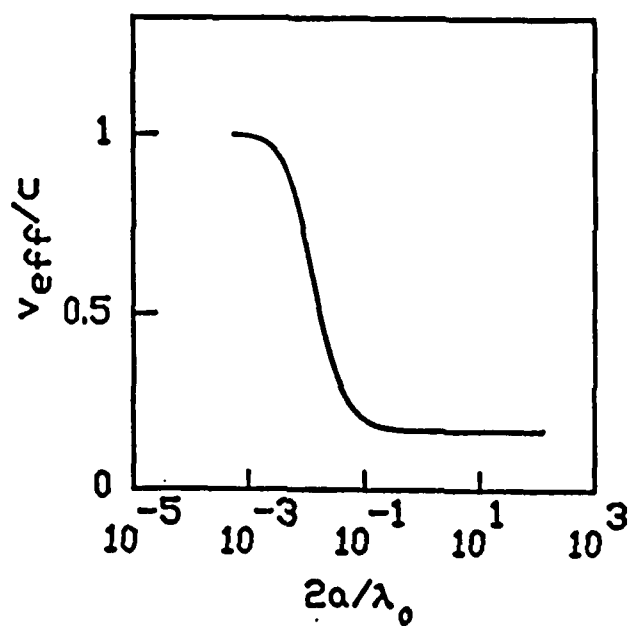


Fig. 4. The relative phase velocity as a function of the design parameter  $2a/\lambda_0$ . Velocity matching can be achieved by having  $2a/\lambda_0 = 0.02$ .



As shown in Fig. 4, the phase velocity is highly dispersive in the region where it can be controlled by the design parameter. In other words, for a given substrate width, velocity matching condition can only be satisfied at a specific modulation frequency. At other frequencies, the velocity matching condition is no longer satisfied. Any modulator based on the H-guide structure, is basically a bandpass-type device. It has a finite bandwidth centered around the design frequency. The bandwidth is, of course, determined by the slope of the dispersion curve, the center frequency, and the length of the device. A 1-cm long device designed at 50 GHz may operate from 40-62 GHz, i. e., the bandwidth is approximately,  $\pm 20\%$ . This is sufficiently large for many application.

In comparison with an integrated optical modulator utilizing coplanar stripline electrodes, the H-guide is expected to have several advantages, namely, better field match between the launching connector and electrodes, larger overlap integral, and true velocity matching. The H-guide has a field pattern similar to the microstripline which is well matched to a cylindrical connector. Because of the better launching condition, one can expect a better frequency response at high frequencies. Since the waveguide is located at the center of the hundred- $\mu\text{m}$ -wide substrate, the modulation field is uniform across the optical waveguide and completely covers the optical waveguide. An overlap integral very close to unity can be achieved. On the other hand, for the coplanar stripline electrodes, a typical overlap integral falls in the range of 0.3-0.5.<sup>7</sup> The H-guide, however, does require more steps in fabrication, i.e., polishing and cutting.

In an H-guide, since the modulation field is rather uniform throughout the electrooptic substrate, one can only make phase modulator or polarization rotator by using a single optical waveguide on the substrate.

Nevertheless, intensity modulation can be obtained by using external components, such as, polarizer, or Mach-Zehnder interferometer.

#### 4. CONCLUSION

In conclusion, we have analyzed the H-guide in detail. We demonstrate that velocity matching can be obtained by properly choosing the width of the substrate. The thickness of the substrate can be made very thin so that the modulation voltage becomes comparable to that of typical waveguide modulators. Because the phase velocity of the modulation signal is dispersive, modulators based on H-guide can't have velocity matching condition satisfied from dc to very high frequencies. They have finite bandwidths. Formulae have been derived for calculating the characteristics of the H-guide.

#### 5. REFERENCES

1. I. P. Kaminow and J. Liu, Proc. IEEE 54, 1374 (1963).
2. P. L. Liu, J. Opt. Commun., 2, 2 (1981).
3. R. C. Alferness, IEEE J. Quantum Electron., QE-17, 946 (1981).
4. S. Korotky and R. C. Alferness, J. Lightwave Tech., LT-1, 244 (1983).
5. L. Thylen and A. Djupsjobacka, J. Lightwave Tech., LT-3, 47 (1985).
6. M. Cohen, in Millimetre and Submillimetre Waves, ed. F. A. Benson, University Microfilm International, Ann Arbor, 1977.
7. P. L. Liu, J. Appl. Phys., 53, 6681 (1982).

### Chapter 3 Design and Layout of Waveguide Modulators Using a Personal Computer

Design and layout of waveguide and electrode patterns are, nowadays, done by using mask design workstations or a mainframe computer with graphical terminals. It involves the use of a software program which can keep track of digitized data points and show the design on a graphical display. When the design of the entire mask pattern is finished, a tape containing the pattern information is generated. The tape is then read by the mask shop and used to drive a mask writing machine. The mask design and layout programs are written for electronic circuits. They are far from ideal for designing waveguide modulators. For example, they can not handle waveguide bends properly. The transverse and longitudinal dimensions of electronic devices are comparable, however, they are very different for waveguides. The transverse dimension of a typical waveguide modulator is in the range of  $10\text{ }\mu\text{m}$  while the longitudinal dimension is in the range of few cm. In addition, there is generally a lack of mask design and layout capability among researchers. It is time-consuming and often subject to errors by having a draftsman to design the mask pattern. Ideally, we need a mask design and layout tool for every engineer who designs optoelectronic devices. The software shall also be customized for designing waveguide devices.

We have indeed developed a software package which runs on personal computers, such as, IBM PC, for the design and layout of mask patterns of waveguide modulators. This package includes pattern fracturing programs and format conversion programs. The pattern fracturing programs can break up any geometry, such as, waveguide bends, Y-junctions, etc., into rectangles with

any given quantization accuracy. The format conversion programs convert data among different pattern description formats. In conjunction with any computer aided design (CAD) tools running on PC, such as, Autocad, our package greatly facilitates the design and layout of waveguide modulators. To our knowledge, we are the first to design and layout waveguide modulators completely on a personal computer.

To demonstrate the use of the pattern fracturing program, we present in Fig. 1 the dialogue between the computer and the user for the design of an S-shaped bend consisting of 6- $\mu\text{m}$ -wide waveguide, a lateral shift of 58  $\mu\text{m}$ , and a length of 6 mm. The quantization accuracy is set at 0.25  $\mu\text{m}$ . Our program automatically breaks up the S-curve and generates a script file which can be read directly by the Autocad to layout the waveguide bend. To reduce the size of the database, only half of the S-bend is digitized. The other half can be generated by placing a mirror image of the first half at the correct location. Placing a mirror image can be done efficiently by using the BLOCK command in Autocad. Similarly, we can design a Y-junction by first fracturing a parallelogram and placing a mirror image of it. Shown in Fig. 2, is a complete waveguide pattern with one Y-junction, a directional coupler, and two S-shaped waveguide bends. As one can notice, there is another major advantage using the Autocad, namely, the magnification factors for the x-axis and y-axis can be different. In the case shown in Fig. 2, the x-magnification factor is 10 while the y-magnification factor is 400. We can see details both in the longitudinal and the transverse dimensions. This feature is not available among conventional mask design and layout tools. After obtaining the waveguide pattern, we can attach the calibration guide and alignment marks to form the mask pattern shown in Fig. 3. After the mask pattern is completely laid out, we can use the DXFOUT command in Autocad to

```

MAS
*** S-CURVE FUNCTION ***

$$Y-Y_0 = -AH * (X-X_0) / BL + AH * \sin(2 * \pi * (X-X_0) / BL) / (2 * \pi)$$

WHERE    AH : HEIGHT
          BL : PERIOD
** PLEASE ANSWER THE FOLLOWING QUESTIONS **
AH=?  BL=?  [ ALL IN UM ]
58,6000
ORIGIN  X=?  Y=?
0,0
LEFTMOST PT  XL=?
0
RIGHTMOST PT  XM=?
3000
RESOLUTION (STEP SIZE) DEL=?
0.25
QUANTIZE STEP SIZE ??  [Y/N]
Y
FILL IN SHAPE ??      [Y/N]?
N
WAVEGUIDE WIDTH  W=?
6
DO YOU LIKE DATA ON SCREEN? [Y/N]
N
PLEASE GIVE A NAME FOR YOUR DATA FILE.....
658.SCR
          -----  END  -----
HA !! YOU HAVE    119 RECTANGLES IN YOUR WORK..
***** YOUR DATA FILE IS ....
        658.SCR
Stop - Program terminated.

C>

```

Fig. 1. The dialogue between the computer and the user for the design of an S-shaped optical waveguide bend. The lateral shift is 58  $\mu\text{m}$ . The length of the bend is 6 mm. Only half of the bend is fractured into rectangles with a quantization step of 0.25  $\mu\text{m}$ .

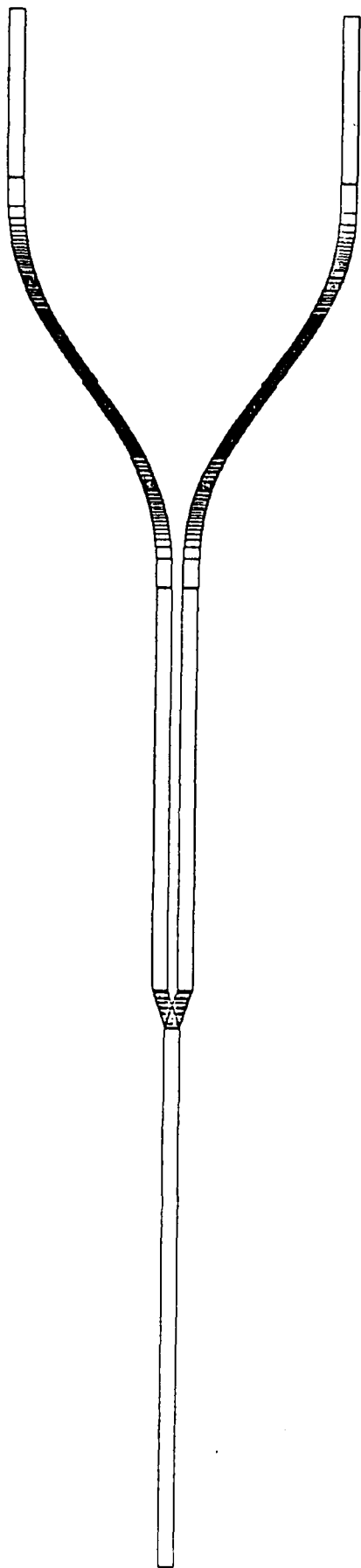


Fig. 2. A complete optical waveguide pattern consisting of a Y-branch, a directional coupler, two S-shaped waveguide bends and input output straight waveguides. The x-magnification is 10 while the y-magnification is 400.

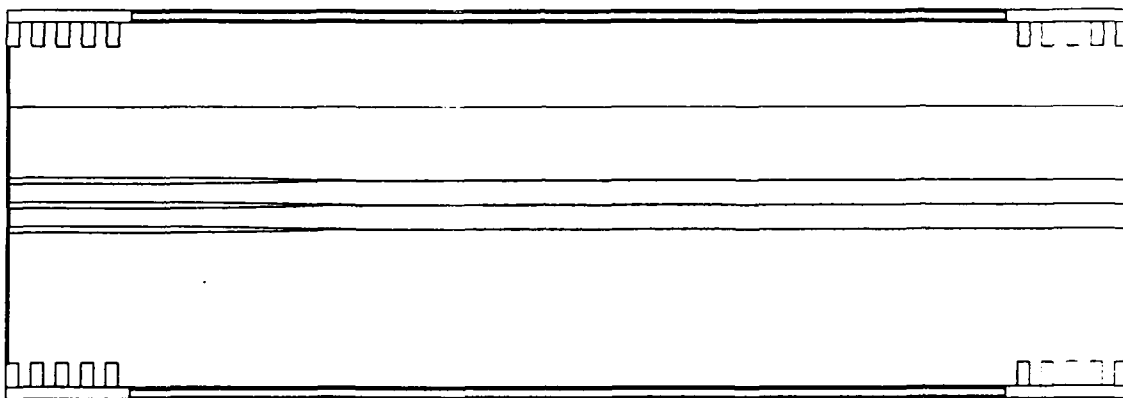


Fig. 3. A mask pattern consisting of a set of three optical waveguide patterns, a straight calibration waveguide, and alignment marks.

generate an ASCII file which completely describes the mask pattern.

In order to transfer the database of a mask pattern to a mask shop, we have developed an automated conversion process. This process converts the output of the Autocad to a Calma GDSII stream. It also back converts from the GDSII to the script file. The back-converted script file can be read by Autocad to re-generate the pattern for comparison. This procedure ensures that there is no error during the conversion process. To further speed up the procedure, we have also developed a line-by-line comparison program which compares the back-converted script file to the original input script file. Any discrepancy is reported on the screen and also recorded in a file. The user does not have to redraw the pattern using Autocad. As long as the back-converted script files are identical to the input files, the conversion process is guaranteed to be error-free.

To demonstrate the above mentioned procedure, we present the dialogue between the computer and the user in Fig. 4 using the database of Fig. 3 as the input. The responses of the user are all underlined. As can be seen, this is an automated batch process. The user answers few questions at the beginning of the batch process. The process then runs its full course automatically. Before the actual conversion process begins, we run a program called LORS which asks whether to use LINE command or the SOLID command in the back-converted script files. Both LINE and SOLID commands can define a rectangle. The LINE command defines the boundary of a rectangle while the SOLID command defines the area of the rectangle. Both of them are converted into the BOUNDARY format in the GDSII stream. In order to carry out the comparison automatically, the operator must inform the computer which command is used in the original script file. The computer then runs a program called DXFCALMA. This program reads in the Autocad database in the



DXF format and converts it into the Calma GDSII format. The operator shall respond to the computer by typing in the name of the DXF file, e.g., YJC1.DXF in this example, and the date. During the conversion process, the computer reports the BLOCK or structure currently being processed on the screen. In this example, we have several building blocks, namely, BASE, BBLOCK, F1, SLANT4, and 658. The pattern shown in Fig. 3 is composed of these building blocks. 658 represents half of the S-shaped bend. SLANT4 represents the

# CONVERT

C>lors

This batch process will convert .dxf file to Calma GDSII.  
It also back converts to Autocad .scr files.  
The back converted files will be compared to the original .scr files.  
This ensures that there is no error during conversion.

Which is in your original .scr file? S(olid) or L(ine)l

C>dxfc alma

File Name for Input: xxxxx.dxf yjcl.dxf  
If you get INPUT PASS END error, there are features other than LINE, SOLID,  
and INSERT in your .dxf file. You have to remove them before running this  
conversion program.

Enter the Date, e.g., 5,8,89 (May 8, 1989)5,25,89

BASE

F1

BBLOCK

SLANT4

658

Total No. of Bytes with Data in GDSII.DB = 10882

The No. of NULL Bytes Patched to GDSII.DB = 1406

C>rename gdsii.db tmp.db

C>patch

The number of bytes is 12288 .

C>search

C>calacad

This file carries a date of 89 - 5 - 25  
The name of the calma file is yjcl.db  
The scale factor is: 1000 Calma units = 1 micron  
One drawing unit in Autocad files equals 1 mm.

level0

BASE

F1

BBLOCK

SLANT4

658

C>compare

BASE

There are 0 lines different.

The number of lines tested is 54 .

F1

There are 0 lines different.

The number of lines tested is 42 .

BBLOCK

There are 0 lines different.

The number of lines tested is 66 .

SLANT4

There are 0 lines different.

The number of lines tested is 126 .

658

There are 0 lines different.

The number of lines tested is 714 .

C>erase clean

C>erase where

C>erase byte

C>erase tmp.db

C>erase sorl

C>

Fig. 4. The dialogue between the computer and the user for the conversion of  
an Autocad database file, YJCL.DXF, to the Calma GDSII stream  
format. The batch process also back converts the GDSII stream  
database to script files and compares them to the original input  
data.

parallelogram in the Y-junction. F1 represents one corner of the alignment frame. BASE consists of the alignment frame and a straight calibration guide. BBLOCK represents the waveguide pattern shown in Fig. 2. After the conversion process is completed, the computer then runs the PATCH program. The Calma GDSII stream uses only full blocks to record the database. Each block has 2048 bytes. The last block of the stream must be filled with nulls to the end of the block. The PATCH program does the filling. At the end of the PATCH program, we generate the GDSII.DB. This is the mask pattern in Calma GDSII format. The rest of the batch process is to ensure that the conversion is error-free.

To ensure that the stream is error-free, we run the back-conversion process from Calma GDSII format to the script file. This is done by first running a SEARCH program. This program searches the GDSII.DB file for any byte with the content of "1A" in hex-representation. This special hex-character is recognized by the program as the end of a file. It has to be replaced before we can run the back-conversion process for the entire database. Without replacing them, the back-conversion program stops prematurely. Since every byte of information counts in the database, we record the location of each appearance of "1A". The actual back conversion is done by the CALACAD program. The back-conversion program, CALACAD, restores "1A" whenever it encounters a byte which has been cleared of "1A". The back-conversion also reports on the screen the structure or BLOCK that it is working on. This program generates a series of script files one for each BLOCK or structure. The next program, COMPARE, takes over. It reads each of the back-converted script file and compares its contents to the corresponding input script file used to compose the mask pattern. It reports any discrepancies on the screen and in a file called LOG. The user does not

have to be present except at the beginning of the automated batch process. After the batch process is completed, the user can type out the LOG file and make sure that there is no error involved. Finally, the batch process erases any temporary file created during the process.

The source codes are written either in BASIC or in C language. They were compiled by IBM Compiled BASIC and C88 compiler. Since each byte counts in the Calma GDSII stream format, we have taken extra care to eliminate any additional byte added by various compilers. For example, the BASIC compiler or interpreter adds "1A" at the end of a file. The Microsoft C compiler patches the end of a file with nulls to make the file length a integer multiple of 128 bytes.

We are the first to generate the GDSII stream database on a personal computer. We want to put mask design and layout tool in the hands of every engineering working of optoelectronic devices and circuits. Since this is a pioneering work, there is no mask shop which can take our GDSII stream database on a floppy diskette at this time. Since to use personal computer is the trend, sometime in the future, the mask shops will be able to read database on a floppy diskette directly. For the time being, we have to go through another procedure, namely, to transfer our GDSII stream database on a floppy to a 9-track tape or a cartridge tape. This can be done by having an outside vendor to copy the file onto a 9-track tape or by transfer the file to a computer with tape drive attached. We have transferred our GDSII stream database to our SUN 4/260 work station. A cartridge tape is generated by running the TAR program under the UNIX operating system on the SUN workstation. This cartridge can be read directly by the mask shop to generate the electron-beam written mask. We have used the KERMIT program in binary format for file transfer from the personal computer to the SUN

workstation. To ensure that there is no error, we have also written a byte comparison program to compare the original database to a file which has been uploaded to and downloaded from the workstation.

In summary, we have written a set of utility programs running on personal computers. We have essentially achieved our goal, namely, to put the mask design and layout capability in the hands of every engineer working of optoelectronic devices and circuits. The user can run any drawing program on a personal computer, which can generate a DXF file. Our utility programs in a batch-processing mode can convert the DXF file into the Calma GDSII stream format. The batch process also verifies that the conversion is error-free by running a back-conversion program and comparing the back-converted script file to the original data line by line.

## Chapter 4 Fabrication Tolerance of $\text{Ti:LiNbO}_3$ Waveguides

So far, fabrication of waveguide modulators are based on trial-and-error. There is no computer aided design tool which can facilitate the design and fabrication of waveguide modulators. We have been engaged in the development of such a tool. For this project, the availability of such a tool is very helpful. We can preview device characteristics.

Simulations of waveguide devices can be carried out similarly to simulations of a high power laser propagating in atmosphere. Based on the index distribution, assuming that the beam is primarily in the forward direction, one can calculate the optical field distribution. Both phase and amplitude information can be obtained. Such an algorithm is called the beam propagation method (BPM). We have developed a BPM code. Our emphasis is on the accuracy of the photonic CAD tool. We compare extensively with previously published device characteristics. Through such an exercise, we are confident that our photonic CAD tool is accurate enough to predict device performance.

Waveguide modulators require highly accurate fabrication techniques. This can be appreciated by simply considering the width of an optical waveguide. A typical stripe guide has a width of  $6\text{ }\mu\text{m}$ . During the photolithography, if the width is missed by half a  $\mu\text{m}$ , the cut-off wavelength, the coupling strength, and the modulating voltage are all changed. In fact, this kind of half-a-micron accuracy must be maintained throughout the entire substrate which is, sometimes,  $50000\text{ }\mu\text{m}$  long. Such a requirement is extremely stringent and is even more so than electronic devices.

With our BPM code, we can predict effects of variations in fabrication conditions on the characteristics of waveguides. From our results, we can put more attention on those crucial parameters during fabrication. We can also try to design devices which are more tolerant to fabrication errors. Our results are summarized in the following manuscript.

## Fabrication Tolerance of Ti:LiNbO<sub>3</sub> Waveguides

### Abstract

A simulation program has been used to study the fabrication tolerance of Ti:LiNbO<sub>3</sub> waveguide devices. Comparisons with measured data and predictions on the performance of new designs are also presented.

### Introduction

The beam propagation method (BPM) [1], is a very useful approach in simulating most guided-wave devices. Based on previously published data on Ti-induced index change and on its dispersion, we have used 3-D BPM to calculate the cut-off wavelengths of the first-order mode from fabrication conditions. The calculated results are consistent with experimental data. We have also calculated the thickness of titanium needed to support the fundamental mode and first-order mode for three Ti-strip widths, 6, 7, and 8  $\mu\text{m}$ .

During the calculation of fabrication conditions for fundamental mode, since the effective indices for the fundamental mode and the higher-order modes are different, we have to use 3-D BPM. However, after using 3-D BPM to ensure that only the fundamental mode is supported, we can then use 2-D BPM to simulate waveguide devices. We have calculated the coupling lengths of Ti:LiNbO<sub>3</sub> directional couplers under different fabrication conditions. Calculated results are consistent with experimental data. The fabrication tolerances of the coupling length of directional couplers are also presented.

### Computation Scheme



#### A. Beam Propagation Method

The propagation of light in a z-cut, y-propagating Ti:LiNbO<sub>3</sub> waveguide is governed by the scalar Helmholtz equation:

$$\frac{\partial^2 E}{\partial x^2} + \frac{\partial^2 E}{\partial y^2} + \frac{\partial^2 E}{\partial z^2} + k^2 n^2(x, z) E = 0. \quad (1)$$

where  $k=2\pi/\lambda$  is the free space propagation constant and  $n(x, z)$  is the refractive index. The electric field can be expressed as

$$E(x, y, z) = E(x, z) \exp(-ikn_b y), \quad (2)$$

where  $n_b$  represents the index of the LiNbO<sub>3</sub> before diffusion. Substituting Eq.(2) into Eq.(1), we obtain the following equation for the complex field amplitude.

$$-\frac{\partial^2 E}{\partial y^2} + 2in(x, z)k \frac{\partial E}{\partial y} = \frac{\partial^2 E}{\partial x^2} + \frac{\partial^2 E}{\partial z^2} + k^2(n^2(x, z) - n_b^2)E. \quad (3)$$

However, instead of finding the eigenvalues and eigenfunctions of Eq.(3), it is sufficient to determine them from the parabolic or Fresnel equation:

$$2in(x, z)k \frac{\partial E'}{\partial y} = \frac{\partial^2 E'}{\partial x^2} + \frac{\partial^2 E'}{\partial z^2} + k^2(n^2(x, z) - n_b^2)E'. \quad (4)$$

The general solutions to Eqs. (3) and (4) can be expressed in terms of the normal-mode eigenfunction expansions:

$$E(x, y, z) = \sum_n A_n u_n(x, z) \exp(-i\beta_n y), \quad (5)$$

$$E'(x, y, z) = \sum_n A'_n u'_n(x, z) \exp(-i\beta'_n y). \quad (6)$$

The normal-mode eigenfunctions for Eqs. (3) and (4) are identical and the normal-mode eigenvalues  $\beta_n$  and  $\beta'_n$  for the same mode index  $n$  are related. Their relationships are:

$$A_n = A'_n, \quad (7)$$

$$u_n(x, z) = u'_n(x, z), \quad (8)$$

$$\beta_n = n_b k \left( \frac{2\beta'_n}{k n_b} - 1 \right)^{1/2}. \quad (9)$$

The BPM solves Eq. (4) by applying the split-operator Fast-Fourier-Transform (FFT).  $E'(x, y+\Delta y, z)$  is formally related to  $E'(x, y, z)$  by

$$\begin{aligned} E'(x, y + \Delta y, z) = & \exp\left(-\frac{i\Delta y}{4n_b k} \nabla_x^2\right) \exp\left(-\frac{in_b k \Delta y}{2} \left(\left[\frac{n(x, y + \Delta y, z)}{n_b}\right]^2 - 1\right)\right) \\ & \cdot \exp\left(-\frac{i\Delta y}{4n_b k} \nabla_x^2\right) E'(x, y, z) + O(y^3). \end{aligned} \quad (10)$$

where  $O(y^3)$  is the error term. The first and the third terms on the right hand side of Eq. (10) can be evaluated by the FFT.

During the calculation of the eigenvalues  $\beta'_n$  and the eigenfunctions  $u'_n$ , the indices without electric-field-induced index change are used. By launching a Gaussian-beam into a single waveguide, we can calculate the spectrum of the following  $y$ -dependent correlation of the complex field:

$$P(y) = \int \int E^*(x, 0, z) E(x, y, z) dx dz. \quad (11)$$

Peaks of the spectrum of  $P(y)$  correspond to the eigenvalues  $\beta'_n$ . The normal-modal eigenfunctions  $u'_n(x, z)$  are obtained by evaluating the following integral for each corresponding  $\beta'_n$ :

$$u'_n(x, z) = 1/Y \int_0^Y E'(x, y, z) w(y) e^{j\beta'_n y} dy. \quad (12)$$

where  $Y$  is the total propagation distance and  $w(y)$  is the Hanning window function. Finally, the eigenfunction of the fundamental mode with unity power is launched into one waveguide of the directional coupler. The power in each waveguide at distance  $y$  is evaluated by calculating the overlap integral of the optical field and the eigenfunction.

#### B. Refractive Index Profile

A Ti:LiNbO<sub>3</sub> waveguide is formed by diffusing a Titanium strip of width  $w$ , and thickness  $\tau$  into a LiNbO<sub>3</sub> substrate. For each waveguide, the Titanium distribution in the substrate after diffusion can be expressed as [4]

$$C(x, z) = 1/2C_0 \exp[-(z^2/4D_z t)] \left[ \operatorname{erf}\left(\frac{w/2 + x}{2\sqrt{D_x t}}\right) + \operatorname{erf}\left(\frac{w/2 - x}{2\sqrt{D_x t}}\right) \right], \quad (13)$$

where  $D_z$  and  $D_x$  are the bulk-diffusion and surface-diffusion coefficients, respectively. The variable  $t$  is the diffusion time.  $C_0$  is the normalization coefficient derived from the following equation:

$$\int_{-\infty}^{+\infty} \int_{-\infty}^{+\infty} C(x, z) dx dz = w\tau, \quad (14)$$

which follows from the law of conservation of matter. The corresponding transverse index profile can be described by

$$n(x, z, \lambda) = n_b(\lambda) + \Delta n(x, z, \lambda), \quad (15)$$

where  $\Delta n(x, z, \lambda)$  is the Ti-induced refractive index change. The relation between  $C(x, z)$  and  $\Delta n(x, z, \lambda)$  is different for TE and TM mode. In addition,

there is a wavelength-dependent dispersion factor. The relationships and values of this factor can be found in Ref.[5].

### C. Effective Index

The 3-D BPM takes large amounts of CPU time to calculate a single result. After knowing that the device supports only the fundamental mode, we can use the 2-D BPM to save computation time. In order to use the 2-D BPM, we must reduce the 2-D transverse indices into 1-D. The approach is to use a single effective index to represent all the indices along the z-direction.

After diffusion, the index in the  $\text{LiNbO}_3$  is

$$n(z) = n_b + \Delta n_s * e^{-z^2/D_B^2}, \quad (16)$$

where  $\Delta n_s(x)$  is the refractive index change at the crystal surface, and  $D_B = \sqrt{(D_z t)}$  is the bulk diffusion length. The effective index for each waveguide mode can be defined by

$$\beta = n_{eff} * k = n_z * k * \cos(\theta), \quad (17)$$

where  $\beta$  is the mode propagation constant, and  $\theta$  is the angle between the wave propagation vector and the y-axis at depth z. A waveguide mode exists only if the total transverse phase shift for one round trip across the guide equals an integral multiple of  $[6]$ , i.e.,

$$2k \int_0^{z_b} [n^2(z) - n_{eff}^2]^{1/2} dz + \Phi_t - \Phi_b = 2m\pi, \quad (18)$$

where  $z_b$  is defined by  $n(x, z_b) = n_{eff}(x)$ , and  $\Phi_t$  and  $\Phi_b$  are the Goos-Hanchen phase shifts corresponding to the total internal reflection at  $z=0$  and  $z=z_b$ . At  $z=z_b$ , the phase shift  $\Phi_b$  for both TE and TM modes are  $-1/2\pi$ , while at  $z=0$ , the phase shifts are

$$\Phi_{TE} = -2 \tan^{-1} \left[ \frac{(n_{eff}^2 - 1)^{1/2}}{(n_s^2 - n_{eff}^2)^{1/2}} \right] \quad (19a)$$

$$\Phi_{TM} = -2 \tan^{-1} \left[ \frac{n_s^2 (n_{eff}^2 - 1)^{1/2}}{(n_s^2 - n_{eff}^2)^{1/2}} \right] \quad (19b)$$

In Eq.(18),  $m=0$  corresponds to the fundamental mode. By substituting Eq.(19) into Eq.(18) and solving the equation, we can get an effective index for each  $x$ . We can then apply 2-D BPM and calculate the results.

We have calculated, for different Ti-strip widths, the cut-off condition for the fundamental mode. The Ti-strip thickness is nominally 750 Å. The diffusion conditions are 1049 °C, 6 hours and 40 min. Fig.1 shows the measured and calculated cut-off wavelengths of the first-order mode. As can be seen, calculated results are in good agreement with measurements. We have also calculated the range of the Ti-strip thickness within which the waveguide is single mode for three different Ti-strip widths, 6, 7, and 8 μm. The diffusion conditions are 1050 °C and 6 hours. The results for TE mode are shown in Fig.2a and the results for TM mode are shown in Fig.2b.

We have used 2-D BPM to calculate the coupling lengths under different fabrication conditions and compared our results to published data by several groups [2],[7]-[9]. All the diffusion conditions are 1050 °C and 6 hours.

The results are listed in Table I. Again, the calculated results are consistent with measured data.

The coupling lengths of the directional couplers are determined by the overlap of the evanescent fields of the two waveguide modes. Any change of the fabrication conditions can change the shape of the waveguide mode and, then, the coupling length. Fig.3 summarizes the calculated result of the change in the coupling length of directional couplers resulting from deviations of fabrication conditions. The nominal pattern of Ti-strip is 6  $\mu\text{m}$  wide and 650 Å thick. The distance between the centers of two waveguides is 12  $\mu\text{m}$ . Devices are diffused at 1050 °C for 6 hours. Under these conditions, the coupling length is 4.76 mm for TM mode, and 3.45 mm for TE mode. Fig. 3a shows the coupling length change as a function of diffusion-temperature change. Fig. 3b is for diffusion-time change. Fig. 3c is for Ti-thickness change. Although the distance between the centers of two waveguides of a directional coupler is fixed, the actual width of Ti stripes, hence, the gap may vary during the fabrication process. Effect of such variations is shown in Fig. 3d using the width of Ti stripes as a parameter. The center-to-center distance is fixed at 12  $\mu\text{m}$ . Fig. 3e is for

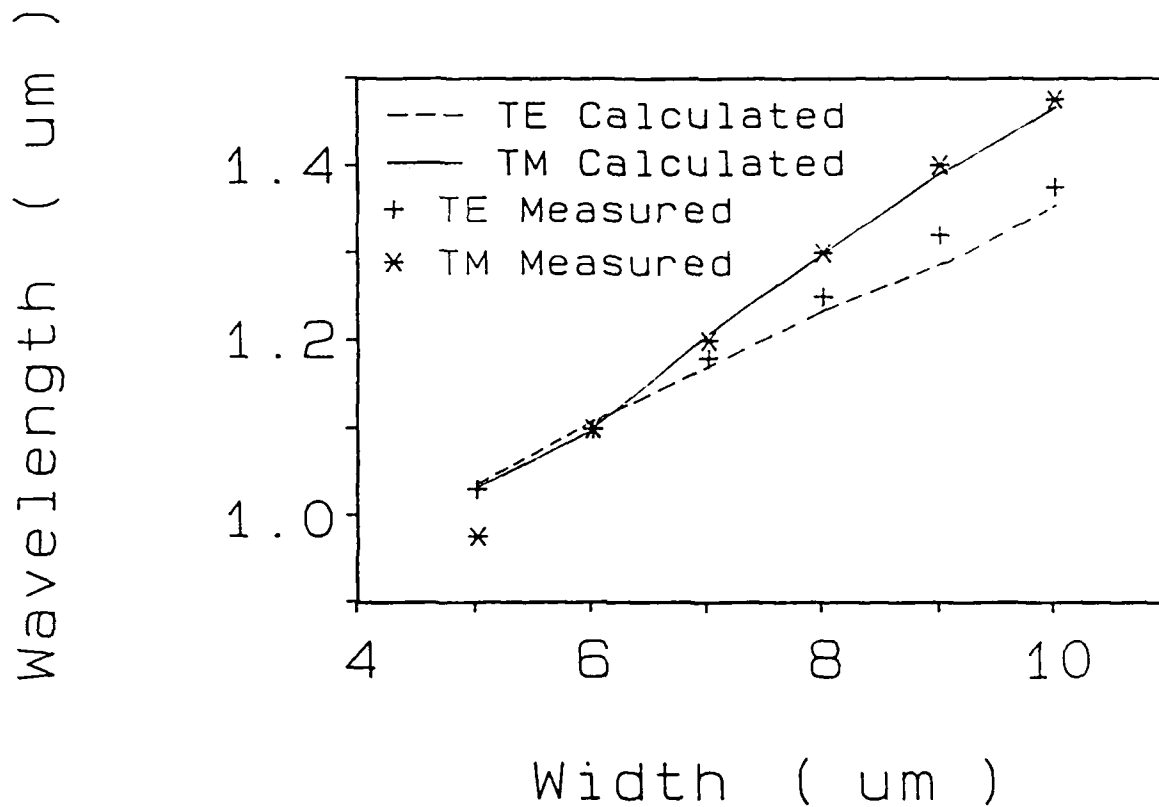


Fig.1 Measured and calculated cut-off wavelengths of the first-order mode of a  $\text{Ti:LiNbO}_3$  guide. The Ti-strip thickness is nominally 750 Å. The diffusion conditions are 1050 °C, 6 hrs and 40 min. Calculated results are linked by solid lines. The results are in good agreement.



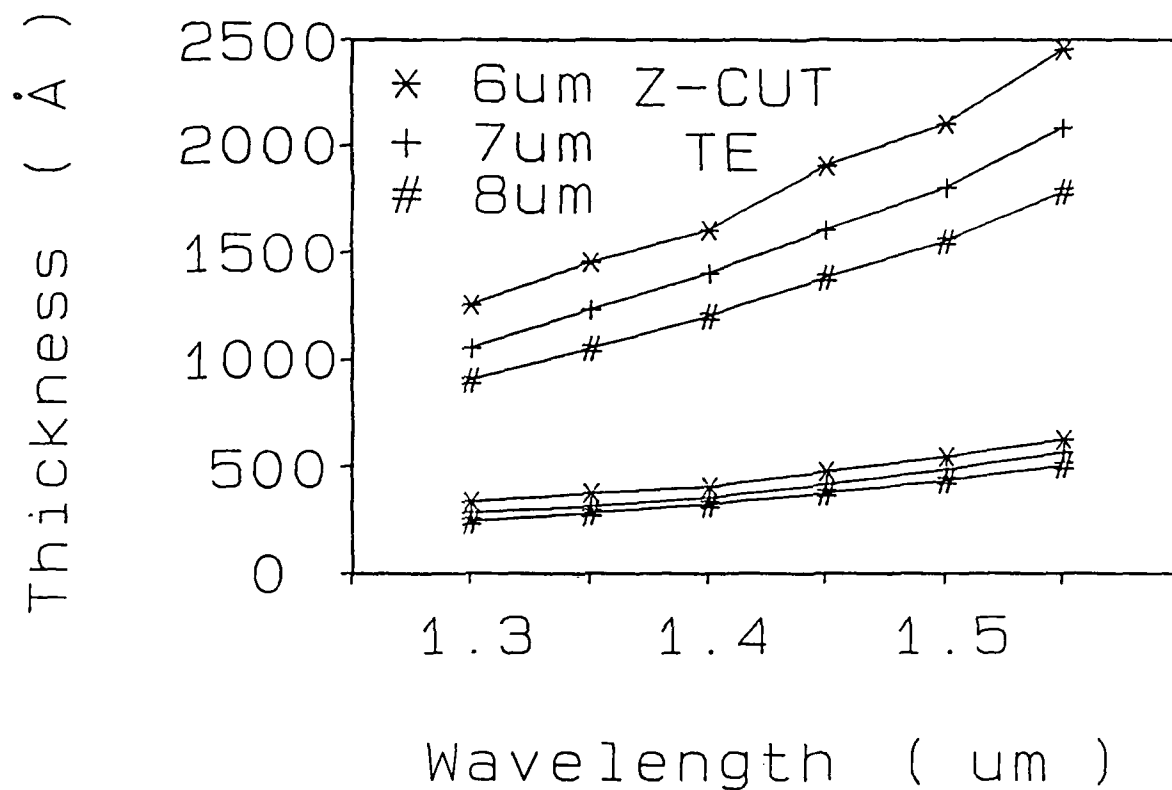


Fig.2 (a) The range of the Ti-strip within which the waveguide is single mode for TE polarization. The diffusion conditions are 1050 °C, 6 hrs. Curves are separated into two groups. The lower group represents the cut-off of the fundamental mode. The upper group represents the cut-off of the first-order mode.

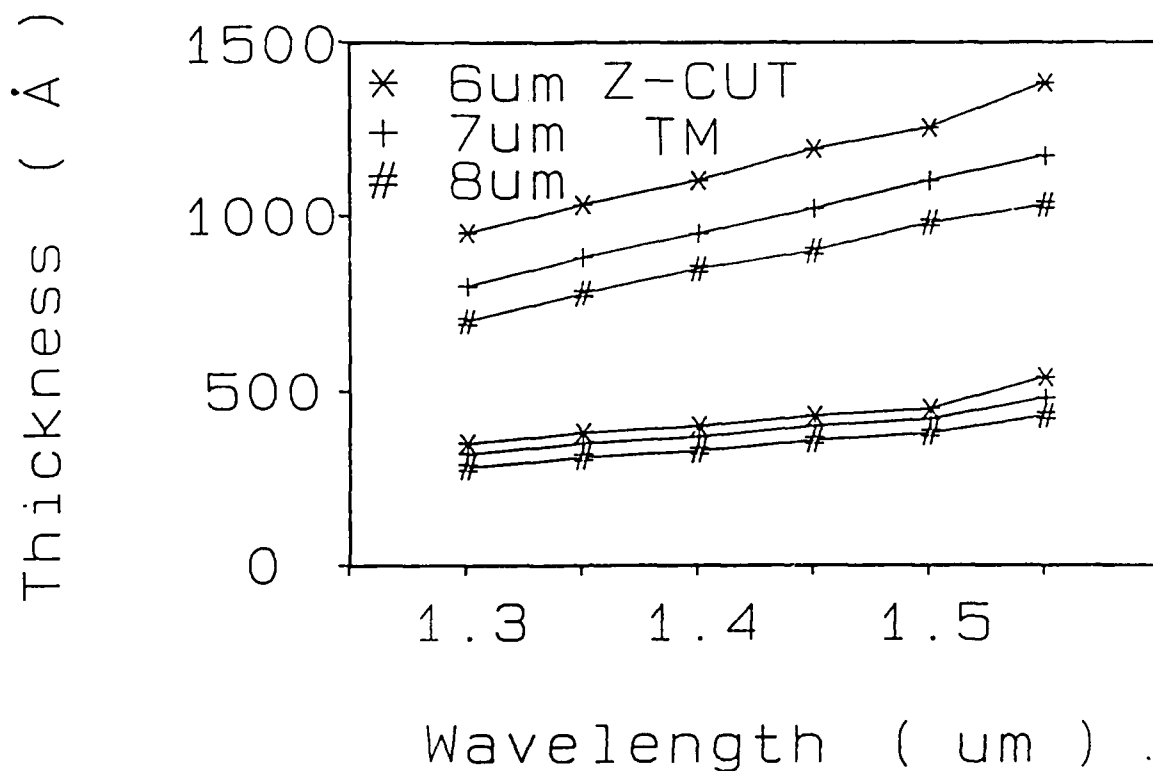


Fig.2 (b) The range of the Ti-strip within which the waveguide is single mode for TM polarization. The diffusion conditions are 1050 °C, 6 hrs. Curves are separated into two groups. The lower group represents the cut-off of the fundamental mode. The upper group represents the cut-off of the first-order mode.

Table I  
Comparison Between Calculation Results and Published Data  
The Diffusion Conditions are 1050 °C and 6 Hours

Wavelength	Polarization	Titanium	Titanium	Waveguide	Calculated	Measured
		Thickness	Width	Separation	Result	Data
( $\mu\text{m}$ )		(Å)	( $\mu\text{m}$ )	( $\mu\text{m}$ )	(mm)	(mm)
1.318	TM	950	6.3	4	3.18	3.1[2]
1.318	TE	950	6.3	4	2.04	2.1[2]
1.3	TM	656	7.4	3.5	2.59	2.5[7]
1.3	TE	656	7.4	3.5	1.87	1.8[7]
1.3	TM	628	7.4	3.7	2.84	2.8[7]
1.3	TM	670	6.5	5	4.23	4.2[8]
1.3	TM	650	6.5	6	6.0	6.1[9]

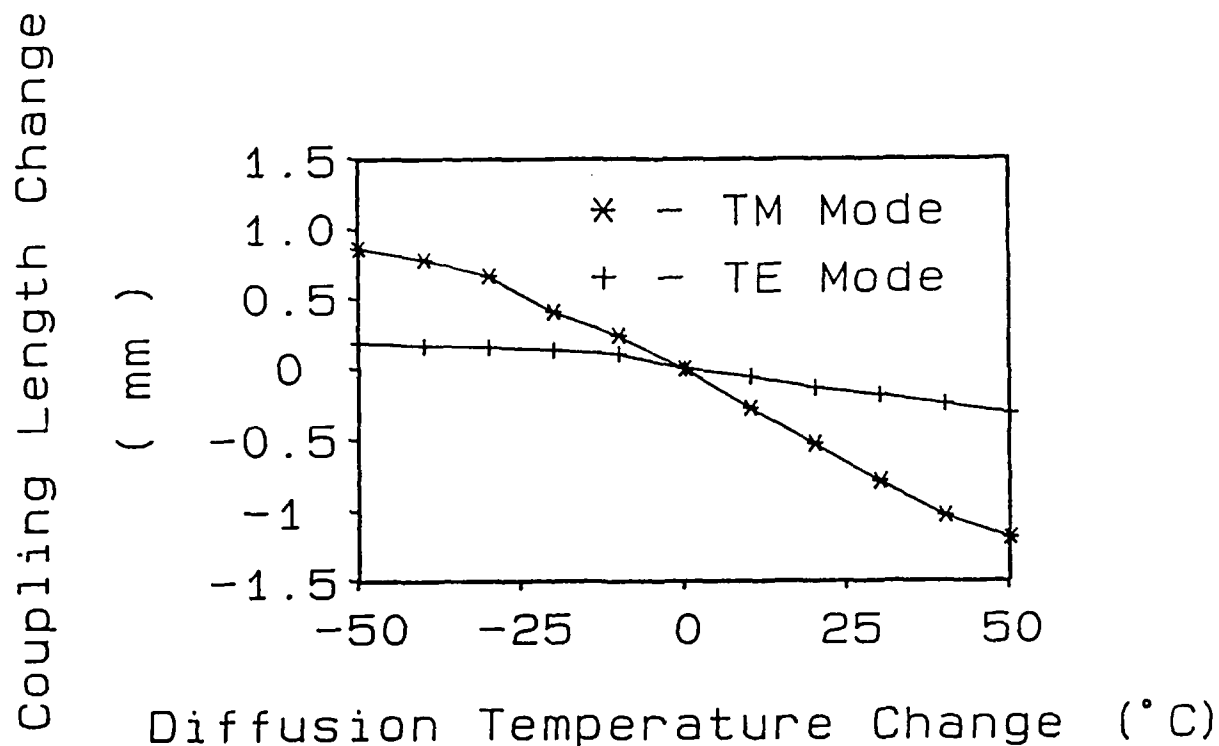
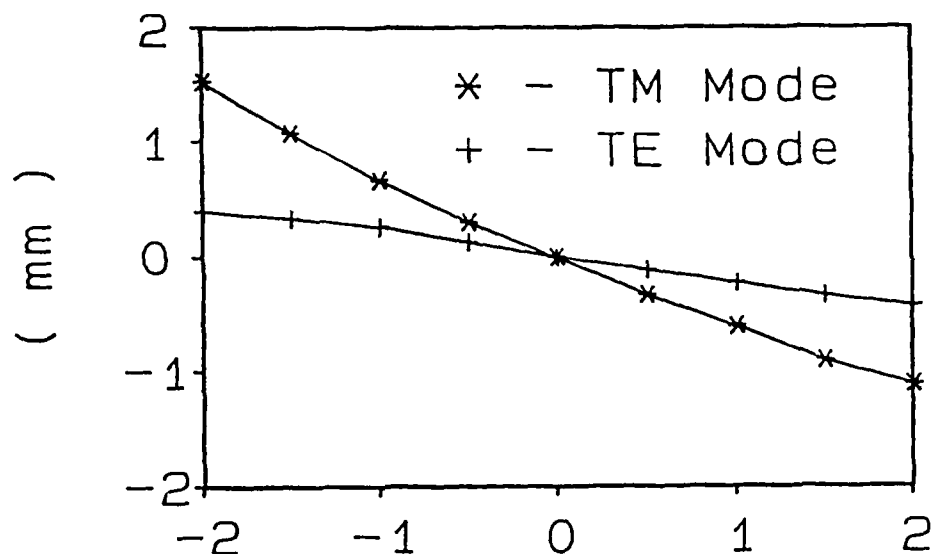


Fig.3(a) The change of coupling length resulting from deviations of diffusion temperature. The nominal conditions for the titanium stripes are  $6\text{ }\mu\text{m}$  wide and  $650\text{ }\text{\AA}$  thick. The distance between the centers of two waveguides is  $12\text{ }\mu\text{m}$ . The diffusion conditions are  $1050\text{ }^{\circ}\text{C}$  and 6 hrs. The coupling length under these conditions is  $4.76\text{ mm}$  for TM mode and  $3.45\text{ mm}$  for TE mode.

Coupling Length Change



Diffusion Time Change ( Hour )

Fig.3(b) The change of coupling length resulting from deviations of diffusion time. The nominal conditions for the titanium stripes are  $6\text{ }\mu\text{m}$  wide and  $650\text{ }\text{\AA}$  thick. The distance between the centers of two waveguides is  $12\text{ }\mu\text{m}$ . The diffusion conditions are  $1050\text{ }^{\circ}\text{C}$  and 6 hrs. The coupling length under these conditions is  $4.76\text{ mm}$  for TM mode and  $3.45\text{ mm}$  for TE mode.

Coupling Length Change  
( mm )

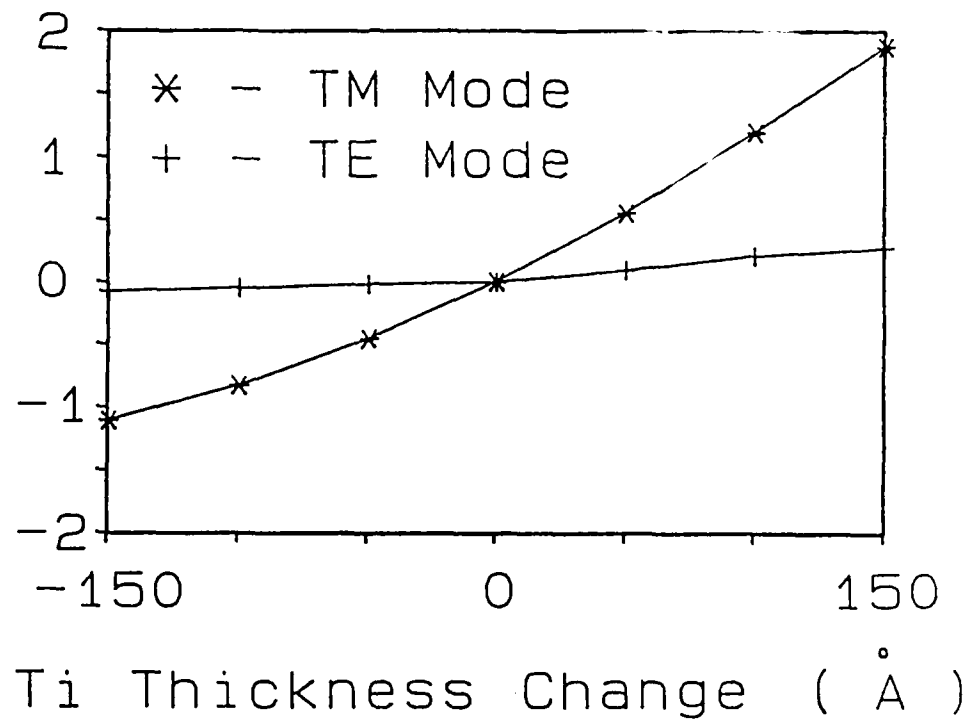


Fig.3(c) The change of coupling length resulting from deviations of Ti thickness. The nominal conditions for the titanium stripes are 6  $\mu\text{m}$  wide and 650 Å thick. The distance between the centers of two waveguides is 12  $\mu\text{m}$ . The diffusion conditions are 1050 °C and 6 hrs. The coupling length under these conditions is 4.76 mm for TM mode and 3.45 mm for TE mode.

Coupling Length Change  
( mm )

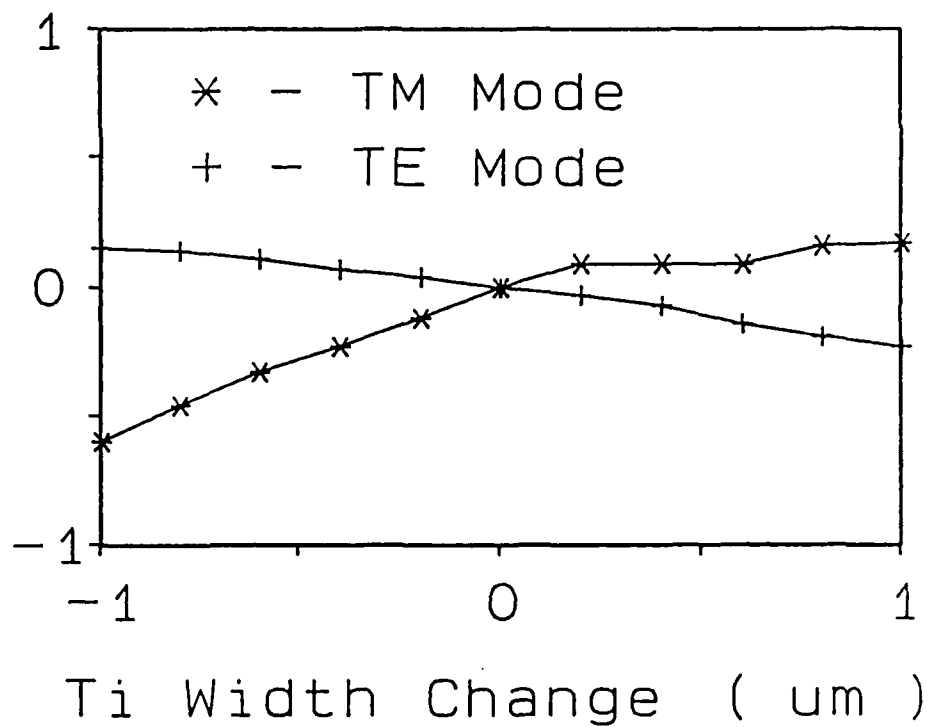


Fig.3(d) The change of coupling length resulting from deviations of Ti stripe width. The nominal conditions for the titanium stripes are 6  $\mu\text{m}$  wide and 650  $\text{\AA}$  thick. The distance between the centers of two waveguides is 12  $\mu\text{m}$ . The diffusion conditions are 1050  $^{\circ}\text{C}$  and 6 hrs. The coupling length under these conditions is 4.76 mm for TM mode and 3.45 mm for TE mode.

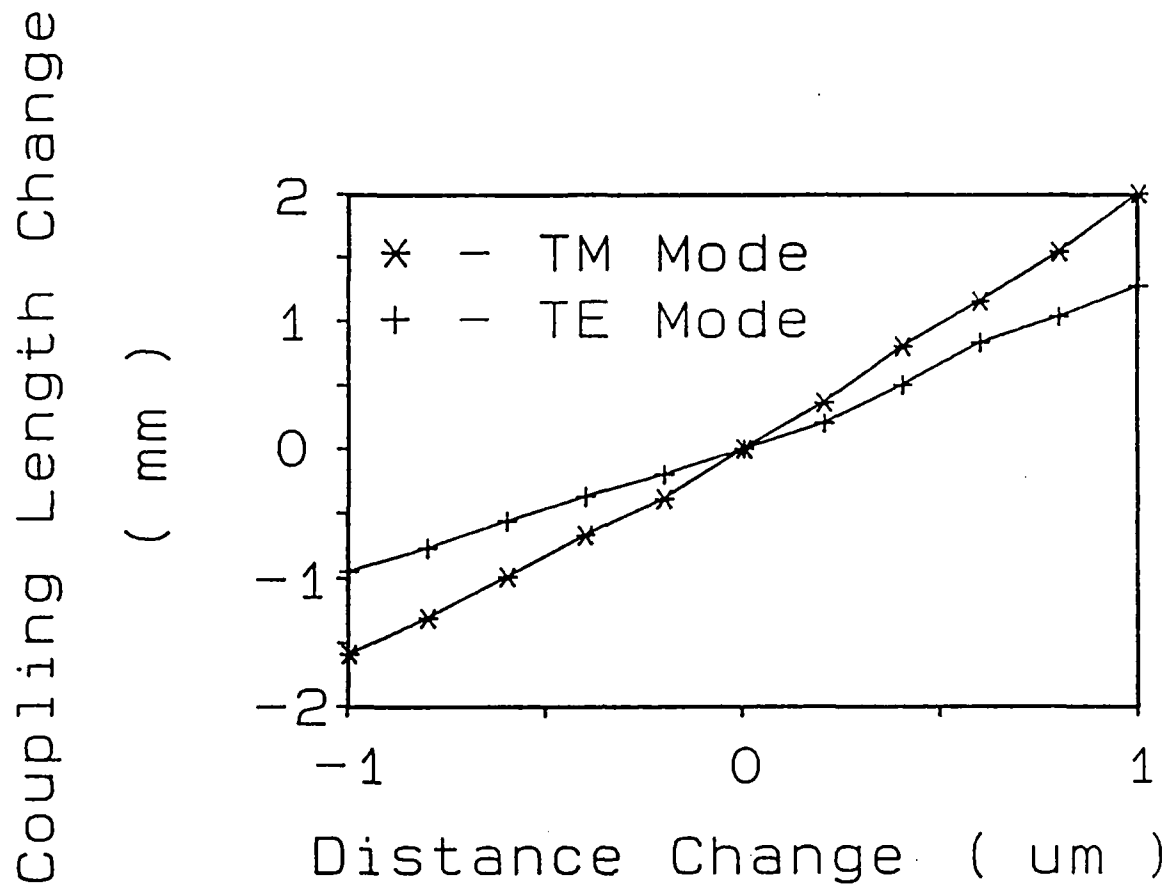


Fig.3(e) The change of coupling length resulting from deviations of distance between two guides. The nominal conditions for the titanium stripes are  $6\text{ }\mu\text{m}$  wide and  $650\text{ }\text{\AA}$  thick. The distance between the centers of two waveguides is  $12\text{ }\mu\text{m}$ . The diffusion conditions are  $1050\text{ }^{\circ}\text{C}$  and 6 hrs. The coupling length under these conditions is  $4.76\text{ mm}$  for TM mode and  $3.45\text{ mm}$  for TE mode.



the center-to-center distance change. Width of waveguides is fixed at 6  $\mu\text{m}$ .

#### Conclusion

A simulation program based on the 3-D BPM has been used to study the fabrication conditions of single-mode  $\text{Ti:LiNbO}_3$  waveguides. The calculated cut-off wavelengths are in good agreement with experimental data. The thickness of titanium needed to support the fundamental mode and first-order mode is calculated for three Ti-strip widths: 6, 7, and 8  $\mu\text{m}$ .

The 2-D BPM is used to calculate the coupling length from the fabrication conditions. Results are consistent with measured data of several groups. The fabrication tolerances of the coupling length of directional couplers are also presented.

## References:

- [1] M.D. Feit and J.A. Fleck, "Computation of Mode Properties in Optical Fiber Waveguides by a Propagating Beam Method," Appl. Opt., Vol. 19, pp.1154-1164, 1980.
- [2] M.D. Feit, J.A. Fleck, and L. McCaughan, "Comparison of Calculated and Measured Performance of Diffused Channel-Waveguide Couplers," J. Opt. Soc. Am., Vol. 73, pp.1296-1304, 1983.
- [3] K. Koai and P.L. Liu, "Modeling of Ti:LiNbO<sub>3</sub> Waveguide Devices: Part I - Directional Couplers," J. Lightwave Tech. Vol. 7, pp. 533-539, 1989.
- [4] M. Fukuma and J. Noda, "Optical properties of titanium-diffused LiNbO<sub>3</sub> strip waveguides and their coupling-to-a-fiber characteristics," Appl. Opt., Vol. 19, pp.591-597, 1980.
- [5] S. Fouchet, A. Carenco, C. Daguet, R. Guglielmi, and L. Riviere, "Wavelength Dispersion of Ti Induced Refractive Index change as a Function of Diffusion Parameters," J. Lightwave Tech., Vol. 5, pp. 700-708, 1987.
- [6] G. B. Hocker and W.K. Burns, "Modes in Diffused Optical Waveguides of Arbitrary Index Profile," IEEE J. Quantum Electronics, Vol. 6, pp. 270-276, 1975.
- [7] L. McCaughan, "Low-Loss Polarization-Independent Electrooptical Switches at  $\lambda=1.3 \mu\text{m}$ ," J. Lightwave Tech., Vol. 2, pp. 51-55, 1984.
- [8] G.A. Bogert, E.J. Murphy, and R.T. Ku, "Low Crosstalk 4x4 Ti:LiNbO<sub>3</sub> Optical Switch with Permanently Attached Polarization Maintaining Fiber Array," J. Lightwave Tech., Vol. 4, pp. 1542-1545, 1986.
- [9] L. McCaughan and G.A. Bogert, "4x4 Ti:LiNbO<sub>3</sub> Integrated-Optical Crossbar Switch Array," Appl. Phys. Lett., Vol. 47, pp. 348-350, 1985.

## Chapter 5 Simulation of Electrooptic Effect on $\text{Ti:LiNbO}_3$ Modulators

In previously published results of BPM, no one has incorporated the electrooptic effect using the actual field distribution. We have considered the actual distribution of the modulating field and found a way to incorporate it in BPM calculations. This is the first attempt to predict details in the characteristics of waveguide modulators. Our results are summarized in the following manuscript.

## Simulation of Electrooptic Effect on Ti:LiNbO<sub>3</sub> Modulators

### Abstract

We have incorporated the electrooptic effect into the 2-dimensional beam propagation method (BPM). We can simulate the modulation characteristics of titanium-indiffused LiNbO<sub>3</sub> devices from fabrication conditions. Directional Couplers with uniform  $\Delta\beta$  and alternating  $\Delta\beta$  electrode configurations are simulated. Results are in good agreement with experimental data found in the literature.

### Introduction

The beam propagation method (BPM) [1], is a very useful approach in simulating most guided-wave devices. In the case of titanium-indiffused LiNbO<sub>3</sub> directional couplers, both 3-D BPM and 2-D BPM can calculate accurately the coupling lengths of the directional coupler from fabrication conditions [2][3]. However, to our knowledge, no one has incorporated the field distribution of the modulation signal into BPM calculations because of the following difficulties. In the case of 3-D BPM, the calculation needs a large amount of memory and computer time. In order to have a reasonable turn-around time, only few points in the transverse plane are sampled and the resolution is poor. After adding the electric-field-induced index change, results may not be accurate owing to the quick change of electric field from one sampling point to another. In the case of 2-D BPM, the B-V curve [4] is widely used to reduce 2-D transverse index to 1-D. However, after adding the electric-field-induced index change to it, there is no longer a closed form for the index along the z-direction and we can't apply it to find the effective indices.

Instead of using the B-V curve, we directly calculate the effective index based on wave optics considerations and then apply the 2-D BPM to simulate the z-cut, y-propagating Ti:LiNbO<sub>3</sub> waveguide devices. From fabrication conditions of the Ti:LiNbO<sub>3</sub> directional couplers and patterns of electrodes, we can calculate the modulation characteristics. Results are in good agreement with experimental data published by several groups.

#### A. Electric Field Calculation

In this paper, we consider symmetric electrodes shown in Fig.1. We assume that the electrodes are infinitely thin. For a z-cut orientation of the LiNbO<sub>3</sub> crystal the potential  $V$  is a solution of the following differential equations

$$\frac{\partial^2 V}{\partial x^2} + \frac{\partial^2 V}{\partial y^2} = 0 \quad \text{for } y > 0, \quad (1a)$$

$$\epsilon_x \frac{\partial^2 V}{\partial x^2} + \epsilon_y \frac{\partial^2 V}{\partial y^2} = 0 \quad \text{for } y < 0, \quad (1b)$$

where  $\epsilon_x=43$  and  $\epsilon_y=28$ . Using the coordinate transformation

$$y' = \frac{\epsilon_x}{\epsilon_y} * y. \quad (2)$$

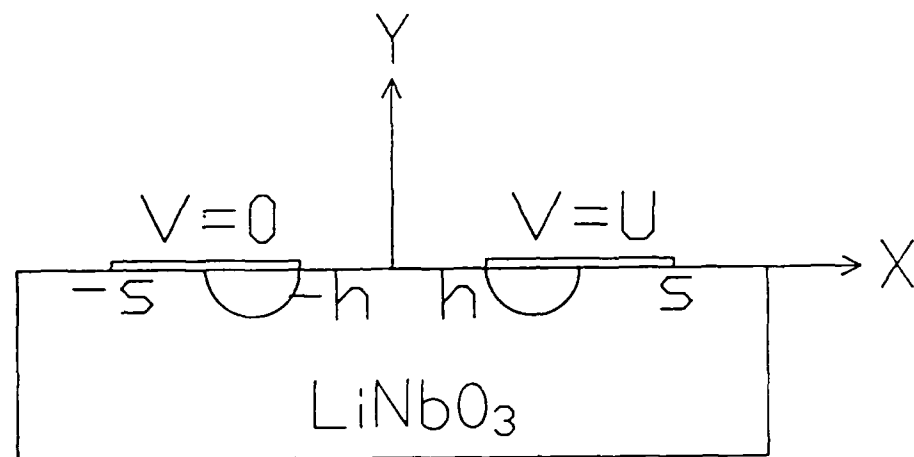


Fig.1 Schematic diagram of the symmetric electrodes fabricated on  $\text{LiNbO}_3$ .

Eq.(1b) can also be written as

$$\frac{\partial^2 V}{\partial x^2} + \frac{\partial^2 V}{\partial y^2} = 0. \quad (3)$$

Therefore, we can just solve Eq. (3). For symmetric electrodes with a width of  $s$ - $h$ , separated by a gap of  $2h$ , the potential can be solved by conformal transformation [7]:

$$z = h * \operatorname{sn}(w, k), \quad (4)$$

where  $z=x+iy$ ,  $w=u+iv$ , and  $k=h/s$ . The potential is given by:

$$V(x, y) = U/2K * [u(x, y') + K], \quad (5)$$

where  $U$  is the voltage and  $K=K(k)$  is the complete elliptic integral of the first kind. The  $x$  and  $y$  components of the electric fields are given by

$$E_x = -\frac{U}{2K} * R\epsilon \frac{dw}{dz}, \quad (6a)$$

(6b)

$$E_y = \sqrt{\frac{\epsilon_x}{\epsilon_y}} * \frac{U}{2K} * \text{Im} \frac{dw}{dz},$$

$$\frac{dw}{dz} = \frac{h}{\sqrt{(h^2 - k^2 z^2)(h^2 - z^2)}}. \quad (6c)$$

## B. Effective Index

The procedures to reduce the 2-D indices into 1-D are :

I. Calculate the index change due to the titanium indiffusion:

$$n(x, z) = n_b + \Delta n_s(x) e^{-z^2/D_B^2}, \quad (7)$$

where  $\Delta n_s$  is the refractive index change at the crystal surface, and  $D_B = 2\sqrt{(D_z t)}$  is the bulk diffusion length.

II. Calculate the index change due to the electro-optic effect.

Since we are now considering z-cut, y-propagating structures, the index change is  $-r_{33}n_b^3 E_y/2$  for TM polarization and  $-r_{33}n_b^3 E_y/2$  for TE polarization. After adding both factors together, the resulting refractive index is

$$n(x, z) = n_b + \Delta n_s(x) e^{-z^2/D_B^2} - r n_b^3 E_y/2. \quad (8)$$

The effective index for each waveguide mode can be defined by



$$\beta = n_{eff}(x)k = n(x,z)\cos(\theta)k, \quad (9)$$

where  $\beta$  is the mode propagation constant, and  $\theta$  is the angle between the wave propagation vector and the y-axis at depth  $z$ . A waveguide mode exists only if the total transverse phase shift for one round trip across the guide equals an integral multiple of  $2\pi$  [4], i.e.,

$$2k \int_0^{z_b} [n^2(z) - n_{eff}^2]^{1/2} dz + \Phi_t + \Phi_b = 2m\pi, \quad (10)$$

where  $z_b$  is defined by  $n(x, z_b) = n_{eff}(x)$ , and  $\Phi_t$  and  $\Phi_b$  are the Goos-Hanchen phase shifts corresponding to the total internal reflection at  $z=0$  and  $z=z_b$ . At  $z=z_b$ , the phase shift  $\Phi_b$  for both TE and TM modes are  $-1/2 \pi$ , while at  $z=0$ , the phase shifts are

$$\Phi_{TE} = -2 \tan^{-1} \left[ \frac{(n_{eff}^2 - 1)^{1/2}}{(n_s^2 - n_{eff}^2)^{1/2}} \right], \quad (11a)$$

$$\Phi_{TM} = -2 \tan^{-1} \left[ \frac{n_s^2 (n_{eff}^2 - 1)^{1/2}}{(n_s^2 - n_{eff}^2)^{1/2}} \right], \quad (11b)$$

In Eq.(10),  $m=0$  corresponds to the fundamental mode. By Substituting Eq.(11) into Eq.(10) and solving the equation, we can get an effective index  $n_{eff}$  for each  $x$ . We can then apply 2-D BPM and calculate the results.

## Results

For the uniform directional coupler, we compared our simulation results to the published experimental data of Murphy et al.[8] and McCaughan et al.[9]. In Murphy's experiment, the light was TM polarized at  $\lambda=1.3\ \mu\text{m}$  and the waveguides were formed by diffusing  $6.5\text{-}\mu\text{m}$ -wide  $670\text{-}\text{\AA}$  thick Titanium stripes at  $1050\ ^\circ\text{C}$  for 6 hours. The directional couplers were  $5.5\ \text{mm}$  long and were separated by  $5\ \mu\text{m}$ . The measured voltage for the bar state ranged from 11.7 to 15.1 volts. Our calculated results are presented in Fig.2

In McCaughan's experiments, the titanium stripes were  $6.5\ \mu\text{m}$  wide,  $650\ \text{\AA}$  thick,  $6.1\ \text{mm}$  long, and were separated by  $6\ \mu\text{m}$ . Again, they were diffused at  $1050\ ^\circ\text{C}$  for 6 hours. At  $\lambda=1.3\ \mu\text{m}$  and TM polarized, their experimental results for bar-state voltages were  $10.5 \pm 1.5\ \text{V}$ . Our calculated results are presented in Fig.3.

For the alternating  $\Delta\beta$  directional coupler, we compare our calculation results to experiments by Murphy [8]. The fabrication conditions are the same. Their measured voltages for the cross state ranged from 6.2 V to 9.7 V. Our calculated results are presented in Fig.4.

We have also simulated the six-section alternating  $\Delta\beta$  directional coupler and compared the results with the experiments from R. V. Schmidt et al.[10]. The wavelength is  $0.6328\ \mu\text{m}$  and TE polarized, waveguides are formed by diffusing  $3\text{-}\mu\text{m}$  wide,  $300\text{-}\text{\AA}$  thick Titanium stripes at  $980\ ^\circ\text{C}$  for 4.5 hours. The waveguides are  $10.5\ \text{mm}$  long and separated by  $3\ \mu\text{m}$ . Their experimental and our calculation results are compared in Fig.5. As we

Crossover Efficiency

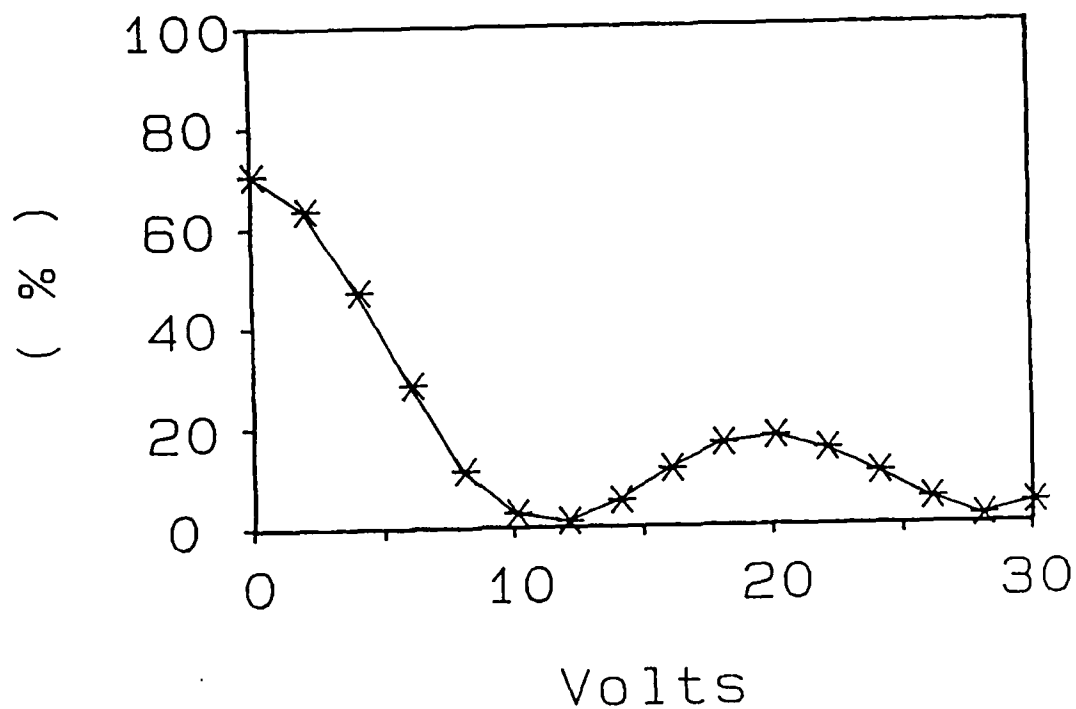


Fig.2 Calculation results of crossover efficiency at  $1.3 \mu\text{m}$ , TM mode. The directional coupler is of uniform  $\Delta\beta$  type and is 5.5 mm long. The Ti-stripes are 670-Å thick,  $6.5\text{-}\mu\text{m}$  wide, and are separated by  $5 \mu\text{m}$ . The diffusion conditions are  $1050^\circ\text{C}$ , 6 hrs. The patterns of the electrodes are  $h=2.5 \mu\text{m}$  and  $s=20 \mu\text{m}$ . Murphy's data for bar state range from 11.7 V to 15.1 V.

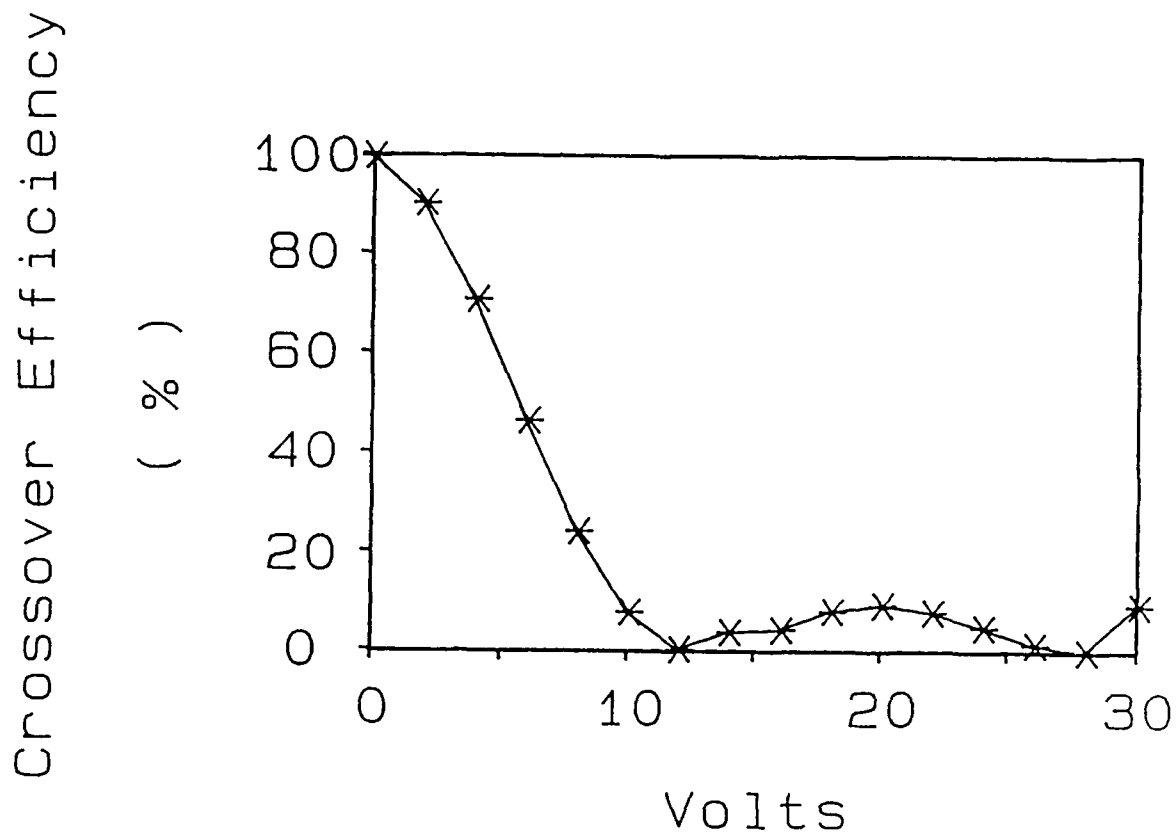


Fig.3 Calculation results of crossover efficiency at  $1.3 \mu\text{m}$ , TM mode. The directional coupler is of uniform  $\Delta\beta$  type and is 6.1 mm long. The Ti-strips are 650-Å thick,  $6.5\text{-}\mu\text{m}$  wide, and are separated by  $6 \mu\text{m}$ . The diffusion conditions are  $1050^\circ\text{C}$ , 6 hrs. The patterns of the electrodes are  $h=3 \mu\text{m}$  and  $s=20 \mu\text{m}$ . McCaughan's data for bar state range from 9 V to 12 V.

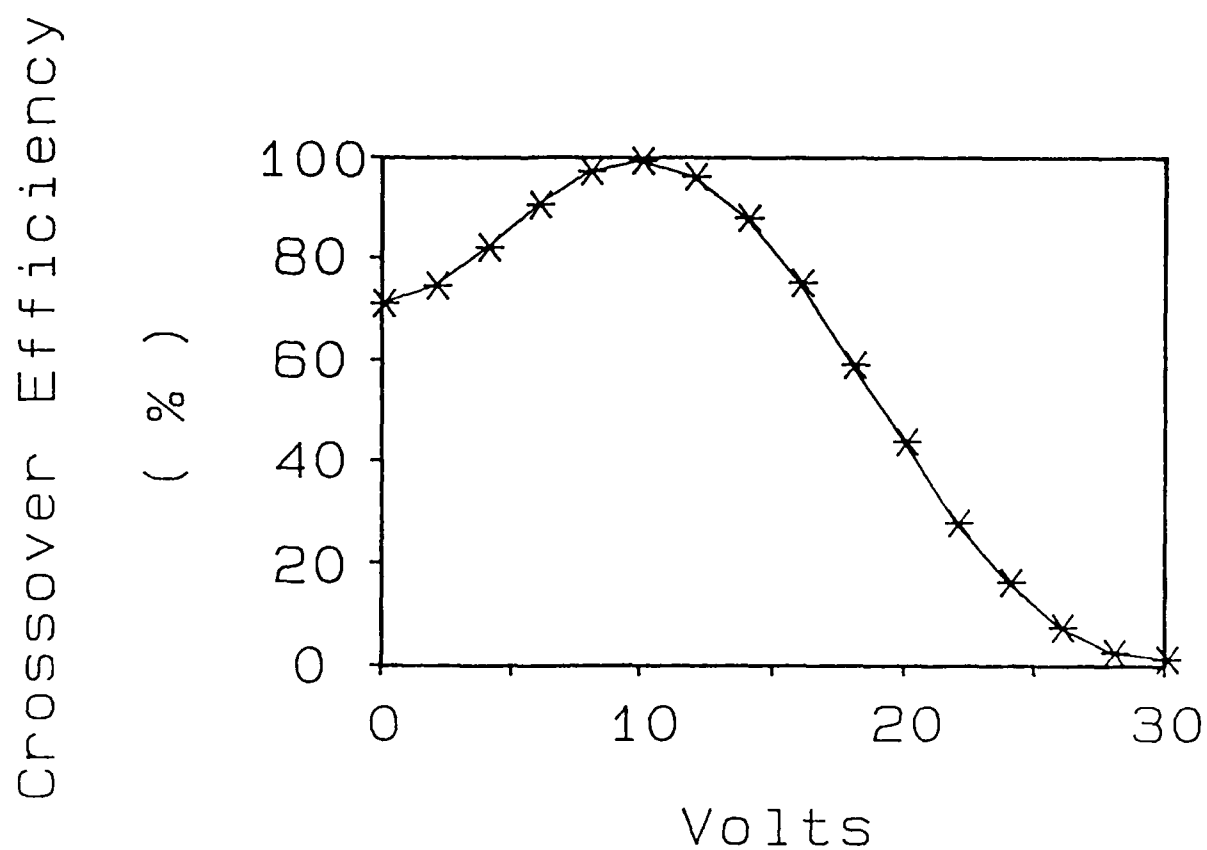


Fig.4 Calculation results of crossover efficiency at  $1.3 \mu\text{m}$ , TM mode. The directional coupler is of alternating  $\Delta\beta$  type and is  $6.1 \text{ mm}$  long. The Ti-stripes are  $670\text{-}\text{\AA}$  thick,  $6.5\text{-}\mu\text{m}$  wide, and are separated by  $5 \mu\text{m}$ . The diffusion conditions are  $1050^\circ\text{C}$ , 6 hrs. The patterns of the electrodes are  $h=2.5 \mu\text{m}$  and  $s=20 \mu\text{m}$ . Murphy's data for cross state range from  $6.2\text{V}$  to  $9.7\text{V}$ .

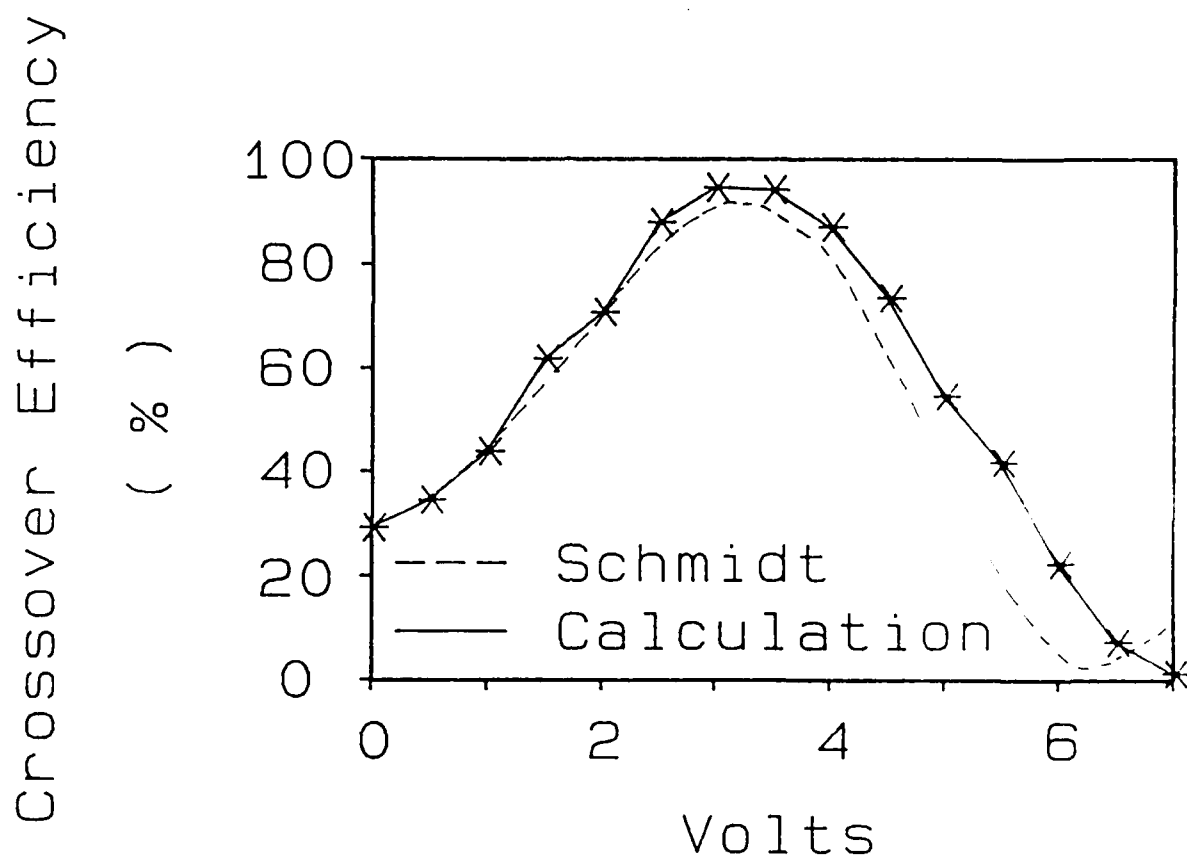


Fig.5 Measured and calculated results of crossover efficiency at  $0.6328 \mu\text{m}$ , TE mode. The directional coupler is of 6-section alternating  $\Delta\beta$  type and is 10.5 mm long. The Ti-strips are 300-Å thick,  $3\text{-}\mu\text{m}$  wide, and are separated by  $3 \mu\text{m}$ . The diffusion conditions are  $980^\circ\text{C}$ , 4.5 hrs. The patterns of the electrodes are  $h=1.5 \mu\text{m}$  and  $s=5 \mu\text{m}$ .

have shown, our calculation results of bar-state voltages for uniform  $\Delta\beta$  directional couplers and cross-state voltages for alternating  $\Delta\beta$  directional couplers fall within the ranges of experimental data. For the six-section alternating  $\Delta\beta$  directional coupler, our calculation results are close to experimental data for the voltages less than 3 V, but there is a systematic discrepancy for voltages greater than 3 V. This may be due to the deviation of electrode patterns from the original design because of fabrication processes.

### Conclusion

We have incorporated the electrooptic effect into the 2-D BPM to simulate the modulation characteristics of  $\text{Ti:LiNbO}_3$  directional couplers. Uniform  $\Delta\beta$ , alternating  $\Delta\beta$ , and six-section alternating  $\Delta\beta$  type electrode configurations are all calculated and compared to published data by several groups. From fabrication conditions and patterns of electrodes, we can accurately calculate the field of the  $\text{Ti:LiNbO}_3$  directional couplers at each position along the propagation direction. Each data point shown in our figures takes less than 5 minutes to calculate on a SUN-4 workstation.

## References:

- [1] M.D. Feit and J.A. Fleck, "Computation of Mode Properties in Optical Fiber Waveguides by a Propagating Beam Method," Appl. Opt., Vol. 19, pp.1154-1164, 1980.
- [2] M. D. Feit, J. A. Fleck, and L. McCaughan, "Comparison of Calculated and Measured Performance of Diffused Channel-Waveguide Couplers," J. Opt. Soc. Am., Vol. 73, pp.1296-1304, 1983.
- [3] K. Koai and P. L. Liu, "Modeling of  $\text{Ti:LiNbO}_3$  Waveguide Devices: Part I - Directional Couplers," J. Lightwave Tech. Vol. 7, pp. 533-539, 1989.
- [4] G. B. Hocker and W. K. Burns, "Modes in Diffused Optical Waveguides of Arbitrary Index Profile," IEEE J. Quantum Electronics, Vol. 6, pp. 270-276, 1975.
- [5] M. Fukuma and J. Noda, "Optical properties of titanium-diffused  $\text{LiNbO}_3$  strip waveguides and their coupling-to-a-fiber characteristics," Appl. Opt., Vol. 19, pp.591-597, 1980.
- [6] S. Fouchet, A. Carencio, C. daguet, R. Guglielmi, and L. Riviere, "Wavelength Dispersion of Ti Induced Refractive Index change as a Function of Diffusion Parameters," J. Lightwave Tech., Vol. 5, pp. 700-708, 1987.
- [7] O. G. Ramer, "Integrated Optic Electrooptic Modulator Electrode Analysis," IEEE J. Quantum Electronics., Vol. 18, pp. 386-392, 1982.
- [8] G. A. Bogert, E. J. Murphy, and R. T. Ku, "Low Crosstalk 4x4  $\text{Ti:LiNbO}_3$  Optical Switch with Permanently Attached Polarization Maintaining Fiber Array," J. Lightwave Tech., Vol. 4, pp. 1542-1545, 1986.
- [9] L. McCaughan and G. A. Bogert, "4x4  $\text{Ti:LiNbO}_3$  Integrated-Optical Crossbar Switch Array," Appl. Phys. Lett., Vol. 47, pp. 348-350, 1985.



- [10] R. V. Schmidt and P. S. Cross, "Efficient Optical Waveguide Switch/Amplitude Modulator," Opt. Lett., Vol. 2, pp.45-47, 1978.

## Chapter 6 Fabrication of Broadband Electrooptic Modulator

The structure of the velocity matched optical transmitter is outlined in Chapter 2 of this report. Our plan is to obtain a 1 cm long, 120  $\mu\text{m}$  wide, and  $<25 \mu\text{m}$  thick  $\text{LiNbO}_3$  substrate with a straight Ti-indiffused waveguide built in. This substrate is sandwiched between two optical flats which are Au plated. The width of the  $\text{LiNbO}_3$  substrate provides the velocity matching. The thin substrate thickness can bring down the modulation voltage.

The first step to make the broadband electrooptic modulator is to thin down the substrate. With a bulk substrate, the modulation voltage is prohibitively high. We have been able to thin substrates down to 25 microns by polishing. The expected modulation voltage is in the range of 10-25 V.

After we fabricate the 6- $\mu\text{m}$  wide, straight Ti: $\text{LiNbO}_3$  waveguide, we thin the substrate from the bottom side. The thinning of the substrate is carried out by using a Logitech high precision polishing jig. The 1 cmx3 cmx1 mm substrate is mounted onto the polishing jig by using Epotek epoxy with the waveguide surface in contact with the mounting block. During mounting, the substrate is pressed against the mounting block until the epoxy completely cures. The mounted substrate is then polished with 600 grit SiC down to 100-150  $\mu\text{m}$ . Both the polishing rate and a gauge attached onto the polishing jig are used to determine the stop time of coarse polishing. If the substrate remains uncracked after coarse polishing, we further polish it with 3  $\mu\text{m}$   $\text{Al}_2\text{O}_3$  particles to as thin as we can without cracking. Usually, the substrate cracks during polishing or during subsequent unmounting. The unmounting is carried out by using a Dynasolve solution to dissolve the epoxy. We have successfully obtained few pieces of 1 cmx1 cmx25  $\mu\text{m}$  substrates. They are cut from the uncracked portion of the original

substrate. Although we have tried to further thin down the substrate, we have not been successful in obtaining pieces with at least 1 cmx1 cm.

In addition to thickness, the transverse dimension of the substrate is also very important. The velocity matching condition can only be met by having the correct transverse dimension, i.e., 120  $\mu\text{m}$ . Since the substrate is too thin for any mechanical procedures by itself, we have to sandwich it between two 1-mm thick glass substrates. A Crystal Bond powder is used as the cement. Crystal Bond powder melts above 120  $^{\circ}\text{C}$ . The two glass substrates are pressed together with a clamp. The clamped sample is then removed from the heater and allowed to cool to the room temperature. After cooling, the Crystal Bond solidifies. The thin  $\text{LiNbO}_3$  substrate is securely protected by the glass substrates. The sandwiched sample is placed on a cutting block using epoxy and cut by a diamond blade saw. The diamond blade saw cuts the sample into stripes of 300  $\mu\text{m}$  to 1 mm. During cutting, we can always obtain 1-mm wide stripes. The 300- $\mu\text{m}$  wide stripes breaks during cutting frequently. After cutting, our sandwiched samples have dimensions of 1 cmx2 mmx300  $\mu\text{m}$ . They are thin and long. They break easily during subsequent treatment. We can not further polish them down to the desirable width. After unsuccessfully experimenting with 300- $\mu\text{m}$  wide stripes, we decide to use the 1-mm wide sandwiched sample for further polishing. Although we can properly mount the sandwiched sample onto the polishing jig, we have not been able to obtain 1 cmx120  $\mu\text{m}$ x25  $\mu\text{m}$   $\text{LiNbO}_3$  pieces. The center  $\text{LiNbO}_3$  always cracks when it is unmounted for examination. It either cracks during polishing or during unmounting. The mechanical rigidity of such a long, thin, and narrow piece of  $\text{LiNbO}_3$  is not strong enough for making devices. Other typical optoelectronic devices, such as, diode laser, have dimensions around 250  $\mu\text{m}$ x250  $\mu\text{m}$ x 200  $\mu\text{m}$ . They look more like a cube. They can be manipulated by

using a vacuum tip. Our samples are thinner and narrower, however, they are 40 times longer. The length makes it impossible to handle.

Parallel with our efforts in polishing and cutting, we have also deposited Au onto optical flats. Optical flats, 1" in diameter, are purchased from Melles Griot. They are chemically cleaned and placed in the evaporator. A 50-Å Ti layer is deposited first to enhance the adhesion and a 700-Å thick Au film is evaporated on the optical flats. The Au layer is further thickened by electro-plating. We have attempted to form an H-guide with 25- $\mu$ m thick substrates. We find that one thin substrate located at the center of the H-guide is not sufficient to maintain the two optical flats parallel. With even a small tilt, the two Au-coated surfaces can be easily shorted. This problem can only be solved by placing two narrow glass stripes with the same thickness and in parallel with the center  $\text{LiNbO}_3$  substrate on the outer edges of the optical flat. The H-guide is, therefore, free from any short. The microwave characteristics are expected to be modified. There are three dielectric stripes in the guide. Since we can feed the H-guide at the center, the effect of the existence of other two dielectric stripes can be minimized by having them placed at least 5 mm away from the center piece. The tail of the microwave field is sufficiently low at such a distance.

Due to the mechanical rigidity of the long, but narrow and thin substrate, we have not been successful in mechanically polishing it down to the right dimensions. Since  $\text{LiNbO}_3$  can not be etched in solution, we can not use any chemical etching process to define the dimensions.

In Fig. 1, we show few of the 25- $\mu$ m thick  $\text{LiNbO}_3$  pieces and stripes obtained after cutting. In Fig. 2, we show the Au-coated optical flat.

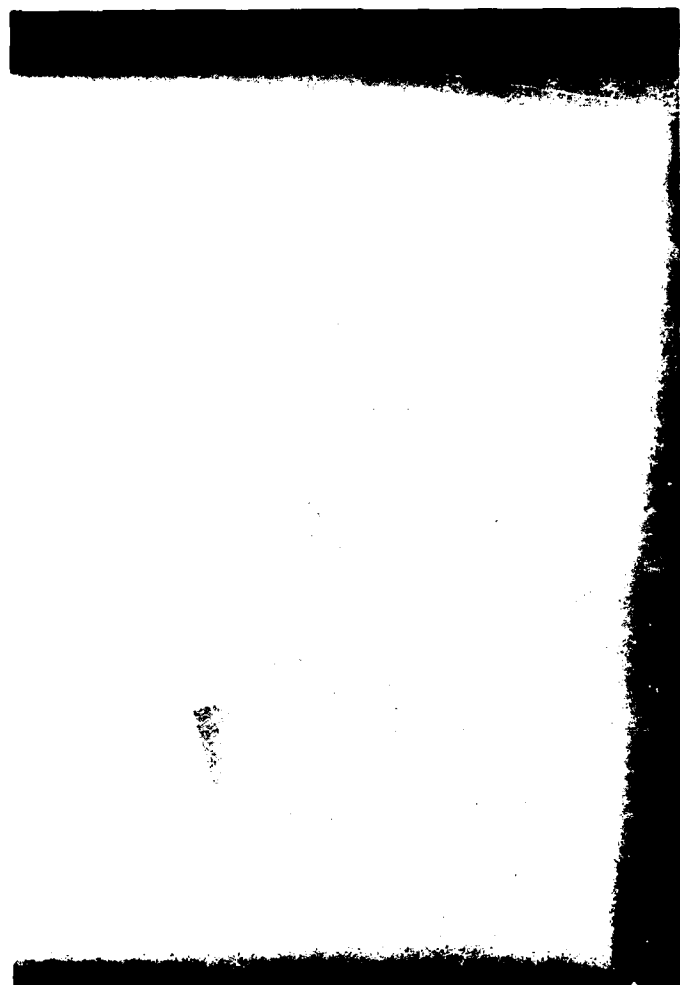


Fig. 1. The 25- $\mu\text{m}$  thick  $\text{LiNbO}_3$  substrates along with stripes cut by using the sandwiched structure to protect the very thin center piece of substrate.

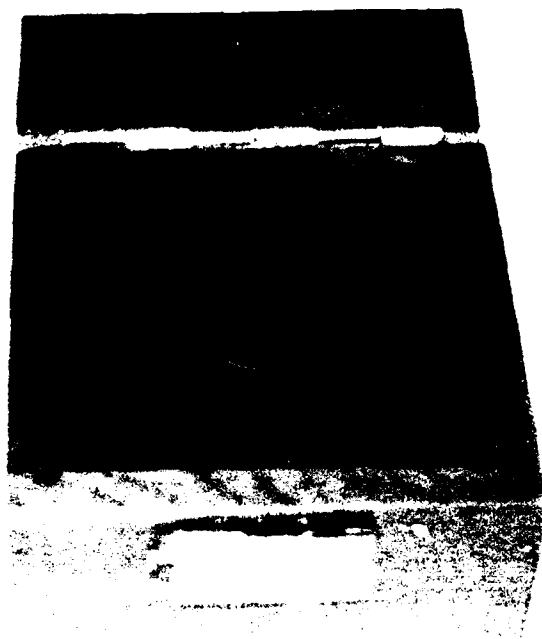


Fig. 2. The Au-coated optical flat.

## Chapter 7 Surface Morphology of Ti:LiNbO<sub>3</sub> Waveguides

Integrated optics is a promising technology. By fabricating optical waveguides and devices on the surface of a substrate, we can make optical integrated circuits. These circuits can control the flow of photons. If a large number of optical circuits with a wide variety of functions can be fabricated on one substrate, such integrated optical chips can be very useful. They can be used in optical switching matrix, high speed signal processing, optical sensors, and possibly in optical computing. As more sophisticated optical communications systems, such as, coherent communications systems, are developed, integrated optical circuits will become more and more important.

A basic requirement for making integrated optical circuits is the ability of forming optical waveguides. Optical waveguides are dielectric guides. A guiding region with a higher index of refraction embeded in the cladding which has a lower index forms the optical waveguide. This index difference can be obtained either by incorporating impurities into the substrate or by changing the material composition. The former is commonly used to make optical waveguides on LiNbO<sub>3</sub> and glass substrates. The later is widely used in compound semiconductors. In the case of LiNbO<sub>3</sub>, Ti-indiffusion and proton-exchange are commonly used to make waveguides. Ti indiffusion can increase both the ordinary and the extraordinary indices of refraction. With properly chosen design parameters and fabrication conditions, both TE and TM modes can be supported. It is the most widely used integrated optical technology. Proton exchange can only increase the extraordinary index of refraction, therefore, only ne mode can be guided.

The Ti indiffusion is typically carried out by diffusing Ti stripe with a thickness ranging from 300 - 750 Å in a wet Ar atmosphere. The typical diffusion temperature used is 1050 °C and the diffusion time is around 6 hrs. Under such diffusion conditions, the diffusion length into the substrate is around 3 μm. From the thickness of the Ti strip and the diffusion length, one can easily find that the Ti concentration in the waveguide region is around 2%. In comparison with impurity level in semiconductor, which is in the range of  $10^{-6}$ , this is very high. With such a high level of impurity, it is hard to imagine that the crystallinity can be maintained. There has been no report on the crystallinity of Ti:LiNbO<sub>3</sub> after in-diffusion. However, there are reports on the scattering of light in the Ti:LiNbO<sub>3</sub> guide. Such scattering has limited the dynamic range of a spectrum analyzer which operates based on the surface acoustic wave. We have also observed the formation of cracks when excess modulation voltage is applied. the surface of the substrate tends to crack along preferred orientation which is at approximately an angle of 45 ° with respect to the length of the waveguide.

In this paper, we report the surface morphology of Ti:LiNbO<sub>3</sub> waveguides. By using an optical confocal microscope, we have observed V-shaped chevron fringes on Ti:LiNbO<sub>3</sub>. Such fringes are stacking faults or microcracks. They lead to increased light scattering and premature breakdown.

Confocal microscope has injected a renewed interest in optical microscopy. The main advantages include increased resolution and the extremely narrow depth of view. In other words, one can monitor a 3-D sample in cross-sections. By using spatial filters, the out-of-focus reflections are rejected. Only a very narrow slice shows up as the image. The increased



resolution comes from the use of a highly monochromatic laser beam as the light source. The beam is raster scanned across the sample surface to form the image. By using the spatial filters, the effect of any lens distortion is suppressed. The resolution is only limited by diffraction. With an objective lens having a large numerical aperture and a short wavelength laser line, a resolution of 2500 Å can be routinely obtained.

The image of a  $\text{Ti:LiNbO}_3$  waveguide directional coupler as observed under a confocal microscope is shown in Fig. 1. The photograph was taken directly from a television monitor. There are two 6- $\mu\text{m}$  wide waveguides. The thickness of the Ti stripes before indiffusion is 650 Å. The diffusion conditions are 1050 °C and 6 hrs. The substrate is a z-cut, y-propagating  $\text{LiNbO}_3$  crystal. The focus of the microscope objective is exactly on the surface of the substrate. The two waveguides are well resolved. Each guide is delineated by two dark bands, one on each side. The brightness in the image is directly related to the local reflection efficiency of the sample. The dark bands along the two sides of the waveguide indicate that the reflection efficiency is reduced along the two sides of a waveguide. This can be explained by the existence of a bulge resulting from Ti-indiffusion. After the indiffusion of the 6- $\mu\text{m}$  Ti stripe, the surface of the substrate is no longer flat. There is a bulge on the surface wherever there is a  $\text{Ti:LiNbO}_3$  waveguide. The central portion of the waveguide is still flat. However, on two edges of the waveguide, there is a slope. Because of the slope, the reflection of the incoming laser beam is directed to the side. It is not reflected back into the collection optics. There is a reduction in the reflection efficiency, hence, a dark band on each side of the waveguide. The two side bands are not perfectly straight. This is a result of residual acoustic vibrations in the confocal optical microscope. The resolution is

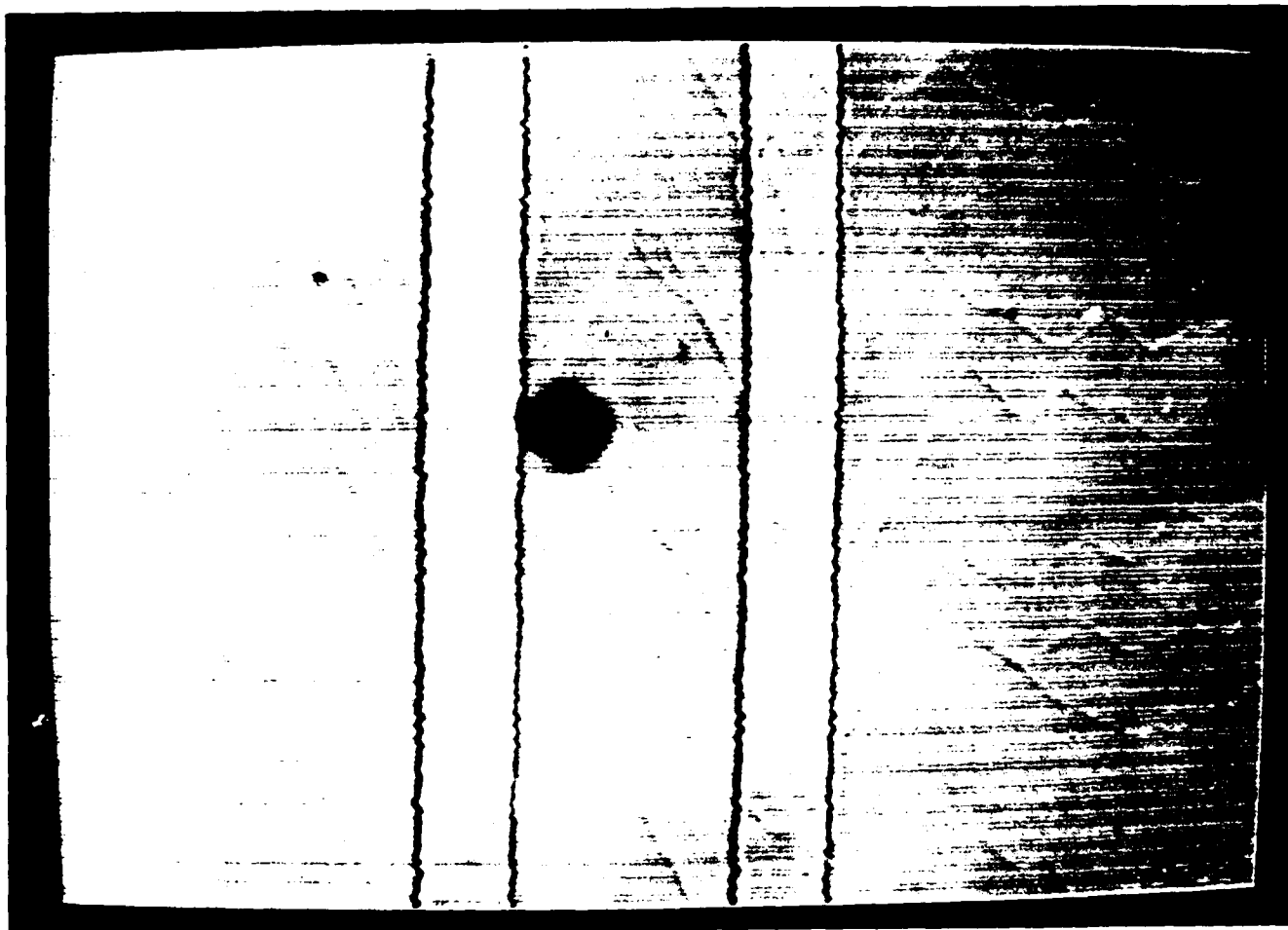


Fig. 1. The surface morphology of  $\text{Ti:LiNbO}_3$  waveguides as observed under an optical confocal microscope.

very high and the beam is scanning, therefore, any residual amount of vibration can show up in the image as a zig-zaged feature.

In addition to the image of waveguides, we can also observe a series of V-shaped chevron fringes with apexes located at the center of the waveguides. These fringes change their courses approximately every 2 -20  $\mu\text{m}$ . They extend to at least few mm away from the waveguide. Since we have a series of parallel waveguides 500  $\mu\text{m}$  apart fabricated on the substrate, these fringes are present on the entire surface of the substrate. These fringes are primarily V-shaped, however, as one can notice, they are not perfectly regular. They, sometimes, bend along the length, i.e., y-axis of the crystal. The angle of the V-shaped chevron is also not a constant. It ranges from 60 to 90°. The black spot near the center of the photograph is an artifact caused by the laser beam.

We have only observed V-shaped fringes on the surface of the substrate where waveguides are present. There is no such fringes on the back side of the substrate. In other words, they are linked to Ti-indiffusion and are not a result of loss of  $\text{Li}_2\text{O}$  which can form planar surface guide. We believe that these fringes are stacking faults or micro-cracks resulting from the incorporation of Ti into  $\text{LiNbO}_3$ . The large concentration of Ti impurity can only be accommodated by an increase in volume. A bulge is developed wherever there is a Ti: $\text{LiNbO}_3$  waveguide. As the bulge forms, stacking faults or microcracks are also formed. They have on the average a preferred orientation and extends well beyond the region where there is a bulge.

To test whether we can eliminate such stacking faults or microcracks, we have fabricated a set of waveguides with diffusion times at 2, 4, 6, and 8 hrs. The Ti thickness is kept constant at 650 Å. The diffusion temperature is also kept constant at 1050 °C. We can not observe any fringes using the confocal optical microscope on samples diffused with a diffusion time

shorter than 4 hrs. They are either not present at all or too small to be seen.

Stacking faults and micro-cracks introduce internal interfaces in the waveguides. They give rise to increased light scattering. The propagational loss is increased and the on-off ratio of a device becomes limited because of stray scattered light. In addition, these micro-cracks weaken the crystal. Under a large modulation voltage, the electric breakdown can occur prematurely along these micro-cracks.

In summary, we have observed, to our knowledge, for the first time, stacking faults or micro-cracks resulting from Ti indiffusion into  $\text{LiNbO}_3$ . They show up as V-shaped chevron fringes on the surface of the substrate under optical confocal microscope. They become too small to be seen if the Ti impurity level is reduced, for example, by reducing the diffusion time. Optical confocal microscopy is a useful, nondestructive method in studying the surface morphology of optoelectronic devices.

## Conclusion

In this project, following progresses have been made:

1. We have thoroughly studied the H-guide configuration and come up with a device design which can operate around 50 GHz.
2. We have developed utility programs so that we can design optical waveguide and electrode patterns using a personal computer.
3. We have further developed our CAD tool for photonic devices. We have incorporated the electrooptic effect and found fabrication tolerances to major fabrication conditions.
4. We have established a fabrication facility for making optoelectronic devices.
5. We have developed procedures to fabricate partially the velocity-matched optical transmitter.
6. We have studied the surface morphology of  $\text{Ti:LiNbO}_3$  waveguides by using an optical confocal microscope.

To meet the velocity-matching condition and maintaining a low modulation voltage, we must cut the substrate into thin, narrow pieces, with following dimensions:  $1 \text{ cm} \times 25 \text{ } \mu\text{m} \times 120 \text{ } \mu\text{m}$ . The substrate becomes too fragile to handle. We have not been able to make a working device so far. Although the operational principle is demonstrated and design parameters obtained, the handling of such a long, thin, and narrow substrate is impractical.

Our findings during this project have been published or submitted. The following is a list of paper and manuscripts:

1. Pao-Lo Liu, "Velocity-Matched Optical Transmitter," Proc. SPIE, vol. 995, 31, (1988).

2. F. S. Chu and P. L. Liu, "Simulation of Electrooptic Effect on  $\text{Ti:LiNbO}_3$  Modulators," submitted to J. Lightwave Tech.
3. F. S. Chu and P. L. Liu, "Fabrication Tolerance of  $\text{Ti:LiNbO}_3$  waveguides," submitted to J. Lightwave Tech.
4. P. L. Liu and P. C. Cheng, "Surface Morphology of  $\text{Ti:LiNbO}_3$  Stripe Waveguides," to be presented in OSA Annual Meeting, 1989.
5. P. L. Liu "Design and Layout of Mask Patterns for Electrooptic Devices on a Personal Computer," to be presented in OSA Annual Meeting, 1989.



## *MISSION of Rome Air Development Center*

*RADC plans and executes research, development, test and selected acquisition programs in support of Command, Control, Communications and Intelligence (C<sup>3</sup>I) activities. Technical and engineering support within areas of competence is provided to ESD Program Offices (POs) and other ESD elements to perform effective acquisition of C<sup>3</sup>I systems. The areas of technical competence include communications, command and control, battle management information processing, surveillance sensors, intelligence data collection and handling, solid state sciences, electromagnetics, and propagation, and electronic reliability/maintainability and compatibility.*